

# Particle generations in $\mathbb{R}^{0|18}$ dust gravity

Robert N. C. Pfeifer\*

*Dunedin, Otago, New Zealand*

(Dated: July 12, 2020)

The  $\mathbb{R}^{0|18}$  dust gravity model contains analogues to the particle spectrum and interactions of the Standard Model and gravity, but with only four tunable parameters. As the structure of this model is highly constrained, predictive relationships between its counterparts to the constants of the Standard Model may be obtained. In this paper, the model values for the masses of the tau, the  $W$  and  $Z$  bosons, and a Higgs-like scalar boson are calculated as functions of  $\alpha$ ,  $m_e$ , and  $m_\mu$ , with no free fitting parameters. They are shown to be  $1776.867(1)$  MeV/ $c^2$ ,  $80.3786(3)$  GeV/ $c^2$ ,  $91.1877(4)$  GeV/ $c^2$ , and  $125.16(1)$  GeV/ $c^2$  respectively, all within  $0.5\sigma$  or better of the corresponding observed values of  $1776.86(12)$  MeV/ $c^2$ ,  $80.379(12)$  GeV/ $c^2$ ,  $91.1876(21)$  GeV/ $c^2$ , and  $125.10(14)$  GeV/ $c^2$ . This result suggests the existence of a unifying relationship between lepton generations and the electroweak mass scale, which is proposed to arise from preon interactions mediated by the strong nuclear force.

## CONTENTS

I. Introduction	1	4. Second-order correction to $K_\ell^4$ from the tau channel	24
II. Boson Mass Interactions	2	5. Dilaton corrections to $\Delta_e(m_{e_i})$	25
A. $W$ mass	2	6. Corrections to $[K_e(\theta_e)]^4$ from the muon and electron channels	25
1. Boson loops	3	IV. Relationships from $\mathbb{R}^{0 18}$ dust gravity	27
2. QL photon and scalar interactions	5	A. Mass relationships	27
3. Universality of loop corrections	6	B. Minimum requirements for particle generations from preon substructure	28
B. $Z$ mass	7	V. Conclusion	29
1. Boson loops	7	A. Gell-Mann matrices	29
2. QL photon and scalar interactions	8	References	29
C. Weak mixing angle	9		
D. Gluon masses	9		
E. Scalar boson mass	10		
1. Vector boson loops	10		
2. Scalar boson loops	11		
F. Neutral boson gravitation	11		
III. Lepton Mass Interaction	12		
A. Leading order	12		
1. Action on colour sector	12		
2. Mass from photon and gluon components of QL	14		
3. Mass from scalar component of QL	15		
4. Gluon and scalar field mass deficits	17		
B. Foreground Loop Corrections	17		
1. 1-loop EM corrections	17		
2. 1-loop gluon corrections	18		
3. 1-loop weak force corrections	20		
4. 1-loop scalar corrections	21		
5. 2-loop EM corrections	21		
C. Corrections to the lepton mass angle	21		
1. Origin of corrections	21		
2. Preamble	21		
3. First-order correction to $K_\ell^4$ from the tau channel	22		

## I. INTRODUCTION

Introduced in Ref. 1,  $\mathbb{R}^{0|18}$  dust gravity is a model comprising a free dust field on the manifold  $\mathbb{R}^{0|18}$ . When this dust field is in a highly disordered and hence (from a coarse-grained perspective) a highly homogeneous state, it admits a description in the low-energy limit where soliton waves in the dust field behave as interacting quasiparticles on a  $\mathbb{R}^{1,3}$  submanifold of  $\mathbb{R}^{0|18}$ . Although the geometry of  $\mathbb{R}^{0|18}$  limits the order of wavefunctions and therefore prevents the dust field from being normalisable on the  $\mathbb{R}^{1,3}$  submanifold, the number of dust particles participating in each quasiparticle is of  $O(10^{36})$ , allowing the effective particles of the low-energy limit to approximate normalisable wavefunctions to order  $O(x^{10^{36}})$ . Fermionic preons condense into leptons, quarks, and a scalar boson, and choices of gauge cause these fields to admit approximate interpretation as normalised particle wavefunctions over a (1,3)-disc submanifold of  $\mathbb{R}^{1,3}$  taken to correspond to the observable universe. Further choices of gauge collapse an emergent  $SU(9)$  symmetry to  $U(1) \otimes SU(2) \otimes SU(3)_C$  while mapping the (1,3)-disc to a region of curved Riemannian space-time denoted  $\tilde{M}$ .

\* rncpfeifer@gmail.com

Breaking of the weak equivalence principle is anticipated, but only in limited domains.<sup>1)</sup>

This paper examines the lepton mass interactions of  $\mathbb{R}^{0|18}$  dust gravity, in which composite leptons acquire mass through coupling to the high-entropy background dust field. On  $M$ , this dust field may be represented as a quantum liquid (QL) described in terms of its non-vanishing expectation values. In the presence of a composite lepton, in the notation of Ref. 1 the familiar non-vanishing bosonic components are

$$\langle [A^\mu(x)A_\mu(y)]_{\text{QL}} \rangle = -\mathbf{f}^{(2)}(x-y) \left[ \mathcal{E}_{\text{QL}}^{(2)} \right]^2 \quad (1)$$

$$\langle [c^{\bar{c}\mu}(x)c_{\bar{c}\mu}^{\bar{c}}(y)]_{\text{QL}} \rangle \Big|_{\bar{c} \in \{1, \dots, 8\}} = -\mathbf{f}^{(2)}(x-y) \left[ \mathcal{E}_{\text{QL}}^{(2)} \right]^2 \quad (2)$$

where  $\mathbf{f}^{(2)}(x)$  is a Gaussian satisfying

$$\int d^4x \left[ \mathcal{E}_{\text{QL}}^{(2)} \right]^4 \mathbf{f}^{(2)}(x-y) = 1 \quad \forall \quad y. \quad (3)$$

These arise from a more general expression

$$\begin{aligned} \langle [\bar{\partial}\bar{\sigma}\partial]_{\bar{c}\mu}^{\dot{m}m} \varphi(x) [\bar{\partial}\bar{\sigma}\partial]^{\dot{n}n\mu} \varphi(y) \rangle & \quad (4) \\ & = -\text{Tr}(e^{\dot{m}m} e^{\dot{n}n}) \mathbf{f}^{(2)}(x-y) \left[ \mathcal{E}_{\text{QL}}^{(2)} \right]^2 \end{aligned}$$

which is written in terms of the underlying dust field  $\varphi$ .

The leptons are made up of three differently-coloured preons, generically

$$\begin{aligned} \Psi^{a\alpha}(x) & \propto (\varepsilon^{\alpha\beta} \varepsilon^{\gamma\delta} - \varepsilon^{\alpha\gamma} \varepsilon^{\beta\delta} + \varepsilon^{\alpha\delta} \varepsilon^{\beta\gamma}) \quad (5) \\ & \times \mathcal{C}_{c_1 c_2 c_3}^g \psi_{\beta}^{t a c_1}(x_1) \psi_{\gamma}^{t a c_2}(x_2) \psi_{\delta}^{t a c_3}(x_3) \end{aligned}$$

where  $g$  is the generation index, and the coefficients  $\mathcal{C}_{c_1 c_2 c_3}^g$  are constrained by requiring that particle  $\Psi^{a\alpha}$  be both colourless and an eigenstate of the mass-generating interaction with the QL. The preon expectation values satisfy

$$\begin{aligned} \langle [\bar{\psi}^{\dot{m}}(x) \bar{\psi}^{\dot{n}}(y) \psi^{\dot{m}}(x) \psi^{\dot{n}}(y)]_{\text{QL}} \rangle & \quad (6) \\ & = \frac{1}{2} \square(\dot{m}, \dot{n}, m, n) \mathbf{f}^{(1)}(x-y) \left[ \mathcal{E}_{\text{QL}}^{(1)} \right]^2 \end{aligned}$$

$$\int d^4x \left[ \mathcal{E}_{\text{QL}}^{(1)} \right]^4 \mathbf{f}^{(1)}(x-y) = 1 \quad \forall \quad y \quad (7)$$

where  $m$  (or  $\dot{m}$ ) and  $n$  (or  $\dot{n}$ ) range from 1 to 9 and enumerate pairs of index values  $a$  (or  $\dot{a}$ )  $\in \{1, 2, 3\}$ ,  $c$  (or  $\dot{c}$ )  $\in \{r, g, b\}$ . The symbol  $\square(\dot{m}, \dot{n}, m, n)$  is defined to equal 1 iff

$$\langle [\bar{\psi}^{\dot{m}}(x) \bar{\psi}^{\dot{n}}(y) \psi^{\dot{m}}(x) \psi^{\dot{n}}(y)]_{\text{QL}} \rangle \quad (8)$$

is an absolute square, and 0 otherwise. Interestingly, the scalar boson is a composite particle made up of preons and satisfies

$$\langle [H'(x)H'^*(y)]_{\text{QL}} \rangle = \frac{9}{2} \mathbf{f}^{(1)}(x-y) \left[ \mathcal{E}_{\text{QL}}^{(1)} \right]^2. \quad (9)$$

In the QL, the field  $A_\mu$  corresponds to the photon, and  $c_{\bar{c}\mu}^{\bar{c}}$  corresponds to gluons associated with the Gell-Mann basis of  $\text{SU}(3)_C$  given in Eq. (A3). The QL introduces a preferred rest frame, but this is largely undetectable at energy scales small compared to  $\mathcal{E}_{\text{QL}}^{(2)}$ , which is comparable to the Planck energy.

Finally, there is also a dilaton field. This is introduced in Sec. III E 1 a of Ref. 1, and is denoted  $\Delta$ . The gradient of the dilaton field,

$$\Delta_\mu = \partial_\mu \Delta \quad (10)$$

acts as a vector boson having no charge with respect to either  $\text{SU}(3)_A$  or  $\text{SU}(3)_C$ . As its QL expectation value has not been zeroed by gauge, by maximisation of entropy in the QL this boson also satisfies a relationship

$$[\Delta^\mu(x)\Delta_\mu(y)]_{\text{QL}} = -\mathbf{f}^{(2)}(x-y) \left[ \mathcal{E}_{\text{QL}}^{(2)} \right]^2. \quad (11)$$

By Eqs. (57–64) of Ref. 1, boson  $\Delta_\mu$  is analogous to vector boson  $\varphi_\mu^{81}$  [1, Eq. (63)], and therefore couples to foreground fields with the same bare interaction strength as the gluons, which are derived from the related bosons  $\varphi_\mu^z|_{z \in \{1, \dots, 80\}}$  of  $\text{SU}(9)$  [1, Sec. III D 1]. The dilaton gradient field may be treated as a ninth gluon, associated with the trivial representation of  $\text{su}(3)_C$ . In what follows, the family of gluons will be taken to include the vector dilaton gradient, giving a combined symmetry group

$$\text{SU}(3)_C \oplus \mathbf{1} \cong \text{GL}(3, \mathbb{R})_C. \quad (12)$$

When referring to uncertainty in results, experimental uncertainties will be denoted  $\sigma_{\text{exp}}$ , and uncertainties in the theoretical calculation will be denoted  $\sigma_{\text{th}}$ .

In this paper, it is generally assumed that any particle under study is at rest or near-rest with respect to the isotropy frame of the QL. It is worth noting that, as per Sec. IV E of Ref. 1, a particle may be considered close to at rest if its boost parameter satisfies

$$\beta < 1 - 10^{32}. \quad (13)$$

## II. BOSON MASS INTERACTIONS

### A. $W$ mass

In Sec. III F 3 of Ref. 1, a first-order expression for the  $W$  boson mass was obtained in terms of two of the free parameters of  $\mathbb{R}^{0|18}$  dust gravity,  $f$  and  $\mathcal{E}_{\text{QL}}^{(1)}$ :

$$m_W^2 = 18f^2 \left[ \mathcal{E}_{\text{QL}}^{(1)} \right]^2 [1 + \text{O}(\alpha)]. \quad (14)$$

To obtain the high-precision numerical results presented in the present paper, it is necessary to evaluate some higher-order corrections to this expression.

<sup>1</sup> For massive bosons, higher-generation leptons, and for normal fermionic matter in regimes with an extremely low two-photon scalar potential—comparable to deep interstellar, perhaps intergalactic space.

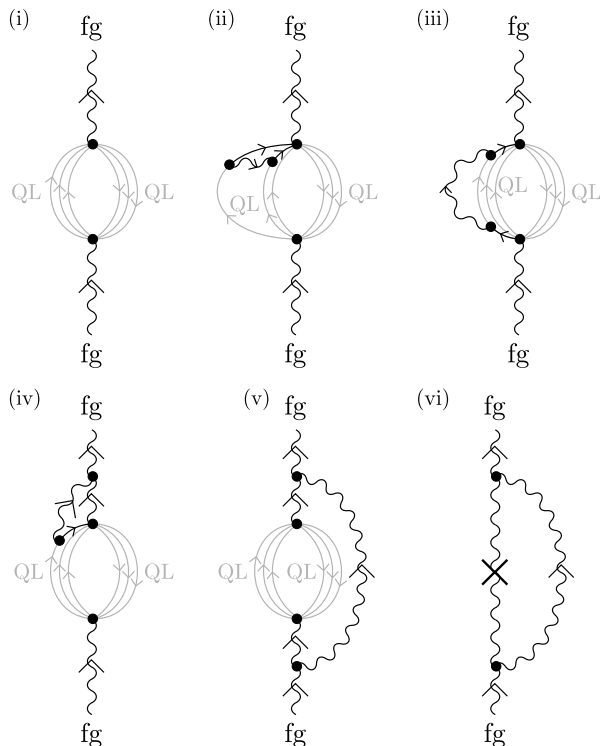


FIG. 1. (i) Leading-order contribution to the  $W$  boson mass. Loop diagrams may (ii)-(iv) modify the  $W$  boson mass-squared interaction, or (v) merely involve it. The Standard Model counterpart to diagram (v) is shown in diagram (vi).

### 1. Boson loops

The leading contribution to the mass of the  $W$  boson arises from interactions between the  $W$  boson and the preon components of the QL. This interaction is corrected by numerous boson loops. When evaluating these corrections, it is important to distinguish between loops which modify the mass-squared interaction, and those which merely involve the mass-squared interaction, as per the examples in Fig. 1.

A diagram is said to “merely involve” the mass-squared interaction if the leading-order interaction of Fig. 1(i) can be replaced by a simple mass vertex  $m_W^2 W^\dagger W$  and the figure in question then obtained from expansion of the propagator in terms of the simple mass vertex and higher-order loop corrections of the Standard Model. Where these same diagrams are present both in the Standard Model and in  $\mathbb{R}^0$ <sup>18</sup> dust gravity, they may be discounted as they do not contribute to calculation of the value of  $m_W^2$  on the mass vertex. (In  $\overline{\text{MS}}$  renormalisation, the mass vertex value of  $m_W^2$  corresponds to the physically observable mass.) An example of such a diagram is Fig. 1(v), with Standard Model counterpart shown in Fig. 1(vi).

Characteristic of the diagrams which do actually modify the mass-squared vertex, and thus impact the value of  $m_W^2$ , is that the loop boson couples to the fermions

which take on QL values in the leading-order diagram of Fig. 1(i). These loops, in turn, may then either (ii-iii) act on a single preon triplet, or (iv) span from that triplet to another part of the diagram. However, once such a loop is introduced, the preons which are evaluated using the QL mean field values no longer all arise from the same vertex. For these preons to remain correlated with their counterparts on the lower vertex, such that the diagram’s contribution to  $m_W^2$  does not vanish, the QL sources and sinks must continue to be within  $O(\mathcal{L}_{\text{QL}})$  of one another, and the loop correction must not introduce any correlations with particles outside the local region (both spatial and temporal) within which the QL is self-correlated. This region has dimensions of order  $\mathcal{L}_{\text{QL}}$ , and is termed the autocorrelation region.

Now recognise that in Figs. 1(ii)-(iii) the loop spans between two components of a composite fermion. These are necessarily separated, on average, by a distance of  $O(\mathcal{L}_\Psi) = O[\mathcal{L}_{\text{QL}}^{(2)}]$ , which is both the length scale associated with fermion mass-squared interactions (as these are quadratic in the QL fields), and the maximum separation of the preon components of a fermion triplet. If the  $W$  boson is at rest in the isotropy frame of the QL, a loop boson propagating between two of these preons will traverse a distance  $O[\mathcal{L}_{\text{QL}}^{(2)}]$  in a time equal to or greater than  $O[c^{-1}\mathcal{L}_{\text{QL}}^{(2)}]$ , depending on whether there are mass interactions along its course. For zero mass interactions a trajectory along the light cone is on-shell, and attracts no mass ratio factor  $\mathbf{f}(m_f^2/m_b^2)$  (for masses of a fermion  $f$  and boson  $b$ ) as the propagating foreground boson is massless in this context. Where mass interactions take place during boson propagation, these slow the propagation of the boson across the distance of  $O[\mathcal{L}_{\text{QL}}^{(2)}]$ . For any non-negligible mass, the time to traverse this distance then exceeds  $O(c^{-1}\mathcal{L}_{\text{QL}}^{(2)})$  causing the ends of the loop correction to no longer both lie within the autocorrelation region for the  $W$  mass interaction. Thus only the light cone trajectory need be considered, and the particles participating in the loop are effectively massless.

Note that this effect (in which particles may appear massless) is only seen in contexts where an observable property is dependent on nonvanishing QL correlators distributed across spatially disparate vertices, and thus under normal circumstances the zero-mass channel is *not* apparent as massless propagation of any particle across a distance large compared with  $\mathcal{L}_{\text{QL}}$  is extremely improbable due to the large number of candidate background QL interactions. Even over a distance of  $O(\mathcal{L}_{\text{QL}})$  there are at least  $O(10^{36})$  such candidate interactions, and the massless channel is only observed when evaluation of the QL preon correlators systematically eliminates the contributions involving massive particles in the loop.

Next, consider Fig. 1(iv) which connects the QL preons to the external  $W$  boson line. This process may take place at arbitrary length scales as connection to the  $W$  boson may take place anywhere along its previous or

subsequent world line. There is no reason for the most heavily-weighted contributions to be those over length scales of  $O(\mathcal{L}_{QL})$  or less, and thus the loop will in general encircle multiple interactions between the  $W$  boson and the QL in the manner of Fig. 1(i). In the absence of any mechanism eliminating interactions over larger length scales, the contributions arising from this diagram sum over all length scales and the long-range couplings introduced by the loop boson thus eliminate sufficient correlations between the QL preon fields to cause the contribution of this diagram to  $m_W^2$  to vanish.

Having thus established (i) that it is only necessary to consider boson loops spanning from one preon to another within a single composite fermion, and (ii) that all bosons in these loops are effectively massless over the length scales involved, these loop corrections may be evaluated as follows:

*a. Gluon loops:* It is convenient to work in the  $e_{ij}$  basis of  $\mathfrak{gl}(3, \mathbb{R})$ . A gluon may arise from one preon and be absorbed by another, as in Fig. 1(ii), or be emitted and absorbed by the same preon as in Fig. 1(iii). Note that the choice of preon propagator to evaluate in the QL mean-field regime in Fig. 1(iii) prevents this diagram being reduced to a foreground self-energy diagram and requires its inclusion in the calculation of  $m_W^2$ .

There are three choices of source preon and three choices of sink preon, for a total of nine gluon loop correction diagrams. By  $GL(3, \mathbb{R})$  symmetry, all of these make equal contributions to  $m_W^2$ . It is convenient to work in the  $e_{ij}$  basis of  $\mathfrak{gl}(3, \mathbb{R})$ , evaluate the correction associated with a gluon which is off-diagonal in colour, and multiply by nine.

For such a diagram, the vertices are each associated with a factor of  $f$ , lasing in the presence of the QL yields a factor of  $\langle N_{QL} \rangle + 1$ , and the definition of a fermion introduces a factor of  $1/3$ . As the boson is off-diagonal, the loop correction attracts a structural factor of  $10/3$  analogous to that seen when calculating the  $W$  boson correction to the electromagnetic anomaly [2], though found to add to, rather than subtract from, the original vertex. A factor of six arises from the admissible permutations of preon colour, but this results in a double-counting on integrating over preon position (corresponding to interchange of both position and colour), reducing this factor to three. The Gaussian integral yields  $1/(2\pi)$ . The net correction associated with this diagram is therefore of weight

$$f^2(\langle N_{QL} \rangle + 1) \cdot \frac{1}{3} \cdot \frac{10}{3} \cdot 3 \cdot \frac{1}{2\pi} = \frac{60\alpha}{9 \cdot 2\pi} [1 + O(\alpha^2)] \quad (15)$$

relative to Fig. 1(i), and the sum over all nine gluon corrections is of weight

$$\frac{60\alpha}{2\pi}. \quad (16)$$

Note that it is not necessary to evaluate a similar set of corrections for the lower vertex: The decision to replace the lower preons in Fig. 1(ii) with the QL mean field

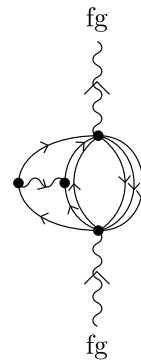


FIG. 2. Underlying diagram which gives rise to Fig. 1(ii) on expansion using mean field theory in the presence of a preon QL.

value is a mathematical one, not a physical one. The base diagram is shown in Fig. 2. If, in evaluating this diagram, the preons above the loop boson were approximated by the QL mean field regime, then the loop boson would yield a correction to the lower vertex, for the same overall result. This yields two equivalent ways to evaluate the same diagram in the presence of the QL to lowest order in the mean field theory expansion, rather than two different physical processes.

*b. Photon,  $W$ , and  $Z$  boson loops:* For the photon, one can proceed as with the gluons, enumerating all the single-preon interactions, or alternatively one can consider a photon loop correction to the fermion as a whole. In this latter approach, consider the interaction between  $W$  boson and leptons, and recognise that a fermion/photon vertex sums over interactions with all three preons and thus automatically enumerates the nine figures described in Sec. II A 1 a. Appropriate selection of preons to evaluate as arising from the QL is assumed. The resulting correction is then immediately seen to be  $\alpha/(2\pi)$ .

For the  $W$ /quark vertex, it is helpful to look at photon/preon interactions and compare these with the  $W$ /lepton vertex. There are numerous ways to count the interactions; one of the simplest is as follows: First, for each vertex recognise that a single-preon photon loop is constructed on the subspace of charged preons. The positions and colours of these preons are immaterial. The subspace is equivalent for the two diagrams, and therefore so is the contribution. Next, consider two-preon photon loops, which occur on the up quark limb for quark vertices, and the electron limb for the lepton vertices. In this case, focus on the subspace corresponding to the participating fermion. For the lepton there are three choices of which pair of preons participates, giving three different locations for the photon loop (three possibilities on one preon configuration). For the up quark there are three choices of preon configuration, with the uncharged preon being in a different location for each, again giving three different locations for the photon loop (one for each of the three configurations). Again there is equivalency.

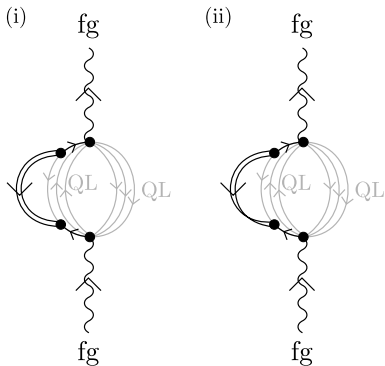


FIG. 3. (i) Scalar boson loop on a fermion propagator. (ii) Crossing of scalar boson constituents.

The electromagnetic factor for the  $W$ /quark vertex is consequently equivalent to that for the  $W$ /lepton vertex.

For  $W$  boson loop corrections a similar approach may be adopted, and it follows immediately from the whole-fermion perspective that since the  $W$  boson is species-changing, no valid  $W$  loop corrections exist.

For  $Z$  boson loop corrections the corresponding interaction weight is

$$-\frac{f_Z \alpha}{2\pi} \quad (17)$$

where

$$\sin^2 \theta_W = 1 - \frac{m_W^2}{m_Z^2} \quad (18)$$

$$\begin{aligned} f_Z &= \frac{1}{3} \left[ (4 \sin^2 \theta_W - 1)^2 - 5 \right] \\ &= \frac{1}{3} \left( 4 - 24 \frac{m_W^2}{m_Z^2} + 16 \frac{m_W^4}{m_Z^4} \right) \end{aligned} \quad (19)$$

and the overall sign reflects that the customary definition of  $f_Z$  is negative, while the  $Z$  and photon terms are additive. By the same argument as in the gluon sector, the  $Z$  boson in the loop is effectively massless over this length scale and thus there is no factor of  $m_f^2/m_Z^2$  for some fermion  $f$ .

*c. Scalar boson loop:* A scalar boson loop may interact with a fermion as shown in Fig. 3(i)-(ii). As in Ref. 1, Sec. III F 4, since the vertex separation is  $\leq \mathcal{L}_\Psi$  the scalar boson constituents may either connect to the vertices collectively as a single composite particle [Fig. 3(i)] or with crossing as shown in Fig. 3(ii). To evaluate Fig. 3(i), recognise that spatially exchanging two preons as in diagram (iii) reveals equivalency to a loop correction arising from a composite vector boson, which is foreground by construction, massless by the same argument as in Sec. II A 1 a, and may be replaced by the equivalent fundamental vector boson using Eqs. (4) and (6) to eliminate the factor of  $[\mathcal{E}_{\text{QL}}^{(2)}/\mathcal{E}_{\text{QL}}^{(1)}]^2$  which accompanies terms in  $H'H^*$ . Following this reduction, the resulting massless foreground boson loop yields a factor of  $\alpha/(2\pi)$ . This is

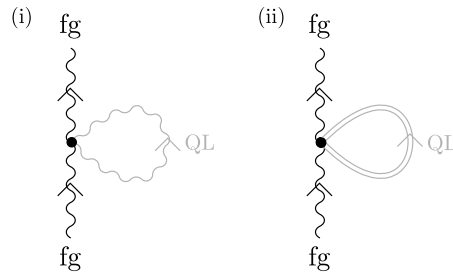


FIG. 4. (i) Coupling between  $W$  boson and QL photon field. (ii) Coupling between  $W$  boson and QL scalar field. For the scalar boson there is no need to separately consider crossed and uncrossed configurations, as all such symmetry factors are incorporated into the mean-squared QL field value.

multiplied by three for the choice of which preon to invert in Fig. 3(i), and by  $[1 + 1/(2\pi)]$  for diagram (ii) by the same arguments as presented in Sec. III F 4 of Ref. 1. The net weight of the scalar boson correction is therefore

$$\frac{3\alpha}{2\pi} \left( 1 + \frac{1}{2\pi} \right). \quad (20)$$

*d. Net effect of all boson loops:* The net effect of the boson loop corrections is therefore to amend the  $W$  boson mass equation to

$$\begin{aligned} m_W^2 &= 18f^2 \left[ \mathcal{E}_{\text{QL}}^{(1)} \right]^2 \left( 1 + \left( 64 + \frac{3}{2\pi} - f_Z \right) \frac{\alpha}{2\pi} \right. \\ &\quad \left. + \text{O} \left\{ \left[ \frac{\mathcal{E}_{\text{QL}}^{(2)}}{\mathcal{E}_{\text{QL}}^{(1)}} \right]^2 \right\} + \text{O}(\alpha^2) \right) \end{aligned} \quad (21)$$

$$f_Z = \frac{1}{3} \left( 4 - 24 \frac{m_W^2}{m_Z^2} + 16 \frac{m_W^4}{m_Z^4} \right) \quad (22)$$

where the next-most-relevant corrections are those due to the coupling of the  $W$  boson to the QL photon and scalar fields, and the second-order electromagnetic corrections.

## 2. QL photon and scalar interactions

Another potentially relevant correction is the  $W$ /QL photon coupling, Fig. 4(i). At tree level this readily evaluates to

$$f^2 \left[ \mathcal{E}_{\text{QL}}^{(2)} \right]^2 \quad (23)$$

where a symmetry factor of 2 arises from the presence of two identical photon operators on the interaction vertex. This gives a net expression

$$\begin{aligned} m_W^2 &= 18f^2 \left[ \mathcal{E}_{\text{QL}}^{(1)} \right]^2 \left\{ 1 + \left( 64 + \frac{3}{2\pi} - f_Z \right) \frac{\alpha}{2\pi} \right. \\ &\quad \left. + \frac{1}{18} \left[ \frac{\mathcal{E}_{\text{QL}}^{(2)}}{\mathcal{E}_{\text{QL}}^{(1)}} \right]^2 + \text{O}(\alpha^2) \right\}. \end{aligned} \quad (24)$$

Inserting the leading-order expressions for  $\mathcal{E}_{\text{QL}}^{(1)}$  (14) and  $\mathcal{E}_{\text{QL}}^{(2)}$  [1, Eq. (192)] into this correction yields

$$m_W^2 = 18f^2 \left[ \mathcal{E}_{\text{QL}}^{(1)} \right]^2 \left\{ 1 + \left( 64 + \frac{3}{2\pi} - fz \right) \frac{\alpha}{2\pi} \right. \\ \left. + \frac{m_e^2}{\left[ k_1^{(e)} \right]^4 m_W^2} [1 + \mathcal{O}(\alpha)] + \mathcal{O}(\alpha^2) \right\} \quad (25)$$

where evaluation of  $\mathcal{E}_{\text{QL}}^{(2)}$  in terms of electron parameters has been chosen as the electron mass is known to the highest precision of the lepton masses. Parameter  $k_g^{(f)}$  is defined in Sec. III A 1, and as in Ref. 1 it is an eigenvalue of the preon colour mixing matrix. However, when proceeding beyond the leading order calculations of Ref. 1 this parameter is seen to run with energy scale. It therefore carries labels  $f$  and  $g$  where  $f$  indicates the family of fermions for which  $k$  is calculated, and  $g$  is the particle generation;  $k_g^{(f)}$  is then eigenvalue  $g$  of the colour mixing matrix  $K_f$  which is associated with the fermion family containing species  $f$ , evaluated at the energy scale  $m_{f_g}$  where  $f_g$  denotes generation  $g$  of the family containing  $f$ . As a matter of notation,  $f$  will generally be taken as the lightest member of the family, and thus (for example)  $k_2^{(e)}$  represents the second eigenvalue of  $K_e$ , evaluated at energy scale  $m_\mu c^2$ .

Energy scale  $\mathcal{E}_{\text{QL}}^{(2)}$  is independent of the particle species used to compute  $m_{f_g}^2 / \left[ k_g^{(f)} \right]^4$ . Using the calculations of the present paper it is only possible to obtain the approximate value

$$\frac{m_{f_g}^2}{\left[ k_g^{(f)} \right]^4} \approx 9.85 \times 10^{16} \text{ eV}^2 / c^4, \quad (26)$$

but this suffices to determine that  $[\mathcal{E}_{\text{QL}}^{(2)} / \mathcal{E}_{\text{QL}}^{(1)}]^2$  lies between  $\alpha / (4\pi)$  and  $\alpha^2 / (4\pi^2)$  in magnitude. Neglecting the correction factor  $[1 + \mathcal{O}(\alpha)]$  on the mass ratio in Eq. (25) introduces errors of  $\mathcal{O}\{\alpha [\mathcal{E}_{\text{QL}}^{(2)} / \mathcal{E}_{\text{QL}}^{(1)}]^2\}$  which are therefore small compared with  $\mathcal{O}(\alpha^2)$  and may be ignored.

The composite QL scalar boson field yields a similar contribution, but:

- Its internal Einstein sum means it receives contributions from nine times as many sectors of the QL, for an additional factor of nine.
- Its internal two-component structure allows for crossed and uncrossed connection of sources and sinks, for an additional factor of two.
- However, the QL field operators on the interaction vertex are no longer interchangeable, for a factor of a half.
- The vertex factor is  $f^2$ , not  $f^2/2$ .

- The Lagrangian term carries an additional factor of  $-2[\mathcal{E}_{\text{QL}}^{(2)} / \mathcal{E}_{\text{QL}}^{(1)}]^2$  by construction.
- The mean field value of  $[H'H'^*]_{\text{QL}}$  is  $-[\mathcal{E}_{\text{QL}}^{(1)}]^2/2$ , compared with  $[\mathcal{E}_{\text{QL}}^{(2)}]$  for  $[AA]_{\text{QL}}$ .

Incorporating the QL scalar boson contribution to  $m_W^2$  therefore yields

$$m_W^2 = 18f^2 \left[ \mathcal{E}_{\text{QL}}^{(1)} \right]^2 \left\{ 1 + \left( 64 + \frac{3}{2\pi} - fz \right) \frac{\alpha}{2\pi} \right. \\ \left. + \frac{19m_e^2}{\left[ k_1^{(e)} \right]^4 m_W^2} + \mathcal{O}(\alpha^2) \right\}. \quad (27)$$

In terms of standard error, the most significant effect arising from the next order of corrections beyond those considered is a contribution to  $m_Z$  at approximately  $10^{-2} \sigma_{\text{exp}}$ , while the largest relative contribution is to  $m_{H'}$  and  $m_Z$ , to approximate order of parts in  $10^7$ . (Note that all attempts to estimate higher-order errors in this paper are approximate, and are determined using the expressions presented in Sec. IV A.)

### 3. Universality of loop corrections

Up to now, the photon in Fig. 4 has been treated as a fundamental particle. However, in principle any occurrence of a fundamental boson may be re-expressed as a pair of preons using the identity

$$\varphi_\mu^{\dot{a}c} = \bar{\partial}^{\dot{a}c} \bar{\sigma}_\mu \partial^{ac} \varphi \approx f \bar{\partial}^{\dot{a}c} \varphi \bar{\sigma}_\mu \partial^{ac} \varphi = f \bar{\psi}^{\dot{a}c} \bar{\sigma}_\mu \psi'^{ac} \quad (28)$$

derived from Eqs. (43) and (80–81) of Ref. 1. Such pairs are bound by the colour interaction with a characteristic separation of  $\mathcal{O}(\mathcal{L}_\Psi)$ , and thus for energies  $\mathcal{E} \ll \mathcal{E}_\Psi$  they appear collocated and at energies small compared to  $\mathcal{E}_\Psi$  this reparameterisation is redundant. However, the length scale  $\mathcal{L}_\Psi$  is comparable to the length scales  $\mathcal{L}_{\text{QL}}^{(1)}$  and  $\mathcal{L}_{\text{QL}}^{(2)}$  associated with mass vertices. The QL fields are characterised by energy scales  $\mathcal{E}_{\text{QL}}^{(k)} = hc / \mathcal{L}_{\text{QL}}^{(k)}$  and thus are capable of discriminating the two constituents when energy is carried in the two-preon mode rather than the fundamental boson mode. Over the length scales associated with mass vertices, this reparameterisation therefore cannot be ignored.

First, consider the preon-mediated mass vertex of Fig. 1(i) and recognise that during evaluation, four of the preon lines are integrated over and eliminated. The remaining two preon lines form a composite vector boson consisting of one preon and one antipreon, and the leading-order expression for  $W$  mass comes from evaluating this in terms of  $\mathcal{E}_{\text{QL}}^{(1)}$  using the fermion sector mean-field theory expression (6). However, it is also valid to

transform the composite vector boson vertices into fundamental boson vertices and obtain a boson loop diagram similar to Fig. 4(i) which gives a coupling to the boson sector expressed in terms of  $\mathcal{E}_{\text{QL}}^{(2)}$ . For the  $W$  boson this contribution vanishes, however, as the resulting QL bosons would be  $W$  or  $W^\dagger$  bosons, and the QL  $W^{(\dagger)}$  fields vanish by gauge except along foreground boson lines [1, Sec. III E 1].

Now consider the diagrams of Fig. 1(ii)-(iii) which contain loop corrections. The preons persisting after integration no longer necessarily arise from the same vertices, but this is unimportant as they are still within  $\mathcal{L}_\Psi$  of one another and can therefore once again be considered to make up a composite vector boson, and thus be mapped to fundamental vector bosons, to again yield a coupling to the boson sector of the QL expressed in terms of  $\mathcal{E}_{\text{QL}}^{(2)}$  (and again these vanish as the bosons are  $W$  bosons). However, now recognise that the inverse process may be applied to any boson loop diagram such as Fig. 4(i), mapping it into a composite vector boson loop and then introducing additional arbitrarily selected preons from the QL. Such a reconstructed six-preon-line diagram then admits loop corrections in the manner described above. This mapping therefore identifies a set of nontrivial higher-order correction to the photon loop diagram of Fig. 4(i) which can only be obtained by mapping the interacting photons into preon constituents and recruiting additional preons from the QL to make up preon vertices.<sup>(2)</sup>

Further recalling that the scalar boson loop in Sec. II A 1 c was evaluated by a mathematical mapping via a composite boson loop to a fundamental boson loop, the converse mapping once again reveals a route back to preon triplet vertices for this diagram, and imparts equivalent corrections to the scalar boson loop diagram of Fig. 4(ii).

The net outcome is that every term in Eq. (21) has a counterpart on the boson loops of Fig. 4, and the  $W$  boson mass may then concisely be written

$$m_W^2 = 18f^2 \left[ \mathcal{E}_{\text{QL}}^{(1)} \right]^2 \left[ 1 + \left( 64 + \frac{3}{2\pi} - f_Z \right) \frac{\alpha}{2\pi} + \mathcal{O}(\alpha^2) \right] \times \left\{ 1 + \frac{19m_e^2}{[k_1^{(e)}]^4 m_W^2} [1 + \mathcal{O}(\alpha)] \right\}. \quad (29)$$

The  $\mathcal{O}(\alpha)$  correction to the term in the second brackets is smaller than the  $\mathcal{O}(\alpha^2)$  term in the first brackets, so

this abbreviates to

$$m_W^2 = 18f^2 \left[ \mathcal{E}_{\text{QL}}^{(1)} \right]^2 \left[ 1 + \left( 64 + \frac{3}{2\pi} - f_Z \right) \frac{\alpha}{2\pi} \right] \times \left\{ 1 + \frac{19m_e^2}{[k_1^{(e)}]^4 m_W^2} \right\} [1 + \mathcal{O}(\alpha^2)]. \quad (30)$$

## B. $Z$ mass

Higher order corrections to the  $Z$  boson mass are also required, and their calculation is similar to that for the  $W$  boson.

### 1. Boson loops

*a. Gluon loops:* The calculation is analogous to that performed for the  $W$  boson. However, introduction of an off-diagonal gluon coupling eliminates the end-to-end symmetry of the  $Z$  boson mass-squared interaction resulting in the loss of a symmetry factor of 2. A similar division by 2 for diagonal gluon couplings is necessary by  $\text{GL}(3, \mathbb{R})$  symmetry, and occurs because replacing the preon line in the loop as in Fig. 1(iii) eliminates interchangeability of the two gluon/preon vertices. The net gluon contribution is therefore

$$\frac{30\alpha}{2\pi}. \quad (31)$$

*b. Photon,  $W$ , and  $Z$  boson loops:* The  $Z$  boson is uncharged, so attracts no net correction from the photon.

Once again, since the  $W$  boson is species-changing, the  $Z$  boson mass diagram also attracts no intra-fermion loop correction involving the  $W$  boson.

For  $Z$  loops, consider the relative contributions of the different fermions which contribute to the leading order diagram [analogous to Fig. 1(i)]. At tree level the  $Z$  boson couples only to electrons, neutrinos, and the down quark family. The relative weights of these contributions to the leading order expression for  $m_Z^2$  are given in the first numerical column of Table I. The coefficients arising from the vertices of the loop correction are given in the second numerical column. The net weight of the  $Z$  boson correction to each channel is the product of these, given in the third numerical column. The total correction arising from  $Z$  boson loops is seen to be

$$\frac{5}{12} \frac{\alpha}{2\pi}. \quad (32)$$

*c. Scalar boson loop:* The scalar boson loop calculation is identical to that for the  $W$  boson, yielding a correction of

$$\frac{3\alpha}{2\pi} \left( 1 + \frac{1}{2\pi} \right). \quad (33)$$

<sup>2</sup> Note that this recruitment (i) is always possible due to the homogeneity of the QL and the extremely large number of QL particles within autocorrelation length  $\mathcal{L}_{\text{QL}}^{(1)}$ , and (ii) is obligatory as the energy scale for a boson at rest in the isotropy frame of the QL mandates that it interacts with triplets.

Species	Weight	Vertex factors	Net loop weight
$e_L^\bullet$	$\frac{1}{8}$	$\frac{1}{6}$	$\frac{1}{48}$
$\bar{e}_R^\bullet$	$\frac{1}{8}$	$\frac{1}{6}$	$\frac{1}{48}$
$\nu_e^\bullet$	$\frac{1}{2}$	$\frac{2}{3}$	$\frac{1}{3}$
$d_L^\bullet$	$\frac{1}{8}$	$\frac{1}{6}$	$\frac{1}{48}$
$\bar{d}_R^\bullet$	$\frac{1}{8}$	$\frac{1}{6}$	$\frac{1}{48}$
Total:	1		$\frac{5}{12}$

TABLE I. List of channels contributing to the leading order  $Z$  boson mass diagram, their relative weights, the vertex coefficients arising when a  $Z$  loop correction is introduced, and the weights of the net contributions of these loop corrections, expressed as multipliers applied to  $\alpha/(2\pi)$ . The net correction arising from  $Z$  boson loops is seen to be  $\{1 + (5/12)[\alpha/(2\pi)]\}$ .

*d. Net effect of all boson loops:* The net effect of the boson loop corrections is therefore to amend the  $Z$  boson mass equation to

$$m_Z^2 = 24f^2 \left[ \mathcal{E}_{\text{QL}}^{(1)} \right]^2 \left( 1 + \left( \frac{401}{12} + \frac{3}{2\pi} \right) \frac{\alpha}{2\pi} \right. \\ \left. + \text{O} \left\{ \left[ \frac{\mathcal{E}_{\text{QL}}^{(2)}}{\mathcal{E}_{\text{QL}}^{(1)}} \right]^2 \right\} + \text{O}(\alpha^2) \right) \quad (34)$$

where the next-most-relevant corrections are those due to the coupling of the  $Z$  boson to the QL scalar field, and the second-order electromagnetic corrections.

## 2. QL photon and scalar interactions

*a. Direct coupling:* As the  $Z$  boson is uncharged, it acquires no mass through direct coupling to the QL photon field. However, it still interacts with the QL scalar boson field. Following a similar calculation to Sec. II A 2 yields

$$m_Z^2 = 24f^2 \left[ \mathcal{E}_{\text{QL}}^{(1)} \right]^2 \left[ 1 + \left( \frac{401}{12} + \frac{3}{2\pi} \right) \frac{\alpha}{2\pi} \right] \\ \times \left\{ 1 + \frac{18m_e^2}{\left[ k_1^{(e)} \right]^4 m_W^2} \right\} [1 + \text{O}(\alpha^2)]. \quad (35)$$

*b. Universality coupling:* Rather surprisingly, however, there does exist a mechanism whereby the  $Z$  boson may acquire mass from the QL photon field. Consider again the mechanism behind the universal applicability of boson mass-squared vertex loop corrections in Sec. II A 3. When the  $Z$  boson is interacting with the preons of the QL, this attracts the obvious leading-order term associated with Fig. 1(i), but when these preons are charged, the residual pair after integration over one set of spatial co-ordinates may then be mapped onto fundamental vector bosons. For charged fermions this mapping results

in a superposition of the photon,  $Z$  boson, and dilaton gradient [which may, in this context, be recruited as a third diagonal boson on  $\text{SU}(3)_A$  as it carries trivial representation on both the  $\text{SU}(3)_A$  and  $\text{SU}(3)_C$  sectors].

Recognising that the off-diagonal fundamental bosons do not contribute to particle mass, only diagonal composite vector bosons need be considered. On-diagonal, for any given composite vector boson with representation matrix  $e_{ii}$  a basis of fundamental bosons may be chosen consisting of the photon,  $Z$  boson, and a boson derived from the dilaton gradient which has a vanishing entry at  $e_{ii}$ . Consequently, any mass arising from this sector may always be attributed to the QL photon field.

First, consider the lepton channels. When the preons are electron-type preons ( $a \in \{1, 2\}$ ) there are three choices of charged preon and three choices of charged antipreon, and freedom to choose which preons to integrate out gives nine ways to make a composite vector boson whose  $a$ -charges indicate it relates to the photon. When the preons are neutrino-type preons ( $a = 3$ ), these have no overlap with the photon and so can be ignored. The lepton sector thus offers a total of 18 channels (nine from  $e_L$  and nine from  $\bar{e}_R$ ).

Next, consider the quark channels. Again, only diagonal contributions from electron-type preons are nonvanishing and thus each down quark contributes only one channel. The up quark does not couple to the  $Z$  boson.

For these twenty channels, now determine the weight of each channel when compared with the  $WW^\dagger AA$  vertex of Fig. 4(i):

- Each channel only constructs half of a photon, either the  $e_{11}$  or the  $e_{22}$  term, for a factor of  $\frac{1}{2}$ . (The overall scaling of the representation matrix is addressed in the next item, in terms of the resulting vertex factor.)
- Vertex and symmetry factors for two couplings of the  $Z$  boson to  $e_L$ ,  $\bar{e}_R$ ,  $d_L$ , or  $\bar{d}_R$  yield a factor of  $\frac{g^2}{8} = \frac{\alpha}{2}$ , compared with  $\frac{g^2}{2} = 2\alpha$  for the  $W$  boson and the photon.
- Given a preon and an antipreon comprising four operators  $ee\bar{e}\bar{e}$  all within a single autocorrelation region, the pairing of  $e$  with  $\bar{e}$  to yield a boson operator is arbitrary, introducing another factor of two in the mapping from composite to fundamental vector bosons.

Summing over all twenty channels, the result is a factor of 5 relative to Fig. 4(i), increasing the  $Z$  boson mass to

$$m_Z^2 = 24f^2 \left[ \mathcal{E}_{\text{QL}}^{(1)} \right]^2 \left[ 1 + \left( \frac{401}{12} + \frac{3}{2\pi} \right) \frac{\alpha}{2\pi} \right] \\ \times \left\{ 1 + \frac{23m_e^2}{\left[ k_1^{(e)} \right]^4 m_W^2} \right\} [1 + \text{O}(\alpha^2)]. \quad (36)$$

It should be noted that no counterpart to the universality coupling applies for the  $W$  boson as its QL preons do

not appear in the correct combinations to be assembled pairwise into components of the composite counterpart to the photon. Also note that when evaluating universality couplings, a choice must be made to work on either the  $SU(3)_A$  or the  $SU(3)_C$  sector. As the  $Z$  boson is associated with a nontrivial representation on  $SU(3)_A$  but a trivial representation on  $SU(3)_C$ , it is necessary to work in the  $SU(3)_A$  sector. Construction of colour-agnostic composite bosons then implicitly spans all valid preon pairs and hence colour choices, making it unnecessary to independently consider the gluon sector.

This completes calculation of  $Z$  boson mass to the level of precision employed in this paper. In terms of standard error, the most significant effect arising from the next order of corrections beyond those considered is a contribution to  $m_Z$  at approximately  $10^{-2} \sigma_{\text{exp}}$ , while the largest relative contribution is to  $m_Z$ , to approximate order of parts in  $10^7$ .

### C. Weak mixing angle

If the weak mixing angle is defined in terms of  $W$  and  $Z$  boson mass, the above results for  $m_W^2$  and  $m_Z^2$  imply a weak mixing angle

$$\begin{aligned} \sin^2 \theta_W &= 1 - \frac{m_W^2}{m_Z^2} \quad (37) \\ &= 1 - \frac{3 \left[ 1 + \left( 64 + \frac{3}{2\pi} - f_Z \right) \frac{\alpha}{2\pi} \right] \left\{ 1 + \frac{19m_e^2}{[k_1^{(e)}]^4 m_W^2} \right\}}{4 \left[ 1 + \left( \frac{401}{12} + \frac{3}{2\pi} \right) \frac{\alpha}{2\pi} \right] \left\{ 1 + \frac{23m_e^2}{[k_1^{(e)}]^4 m_W^2} \right\}} \\ &\quad \times [1 + \mathcal{O}(\alpha^2)] \quad (38) \end{aligned}$$

where  $f_Z$  in turn depends on  $\sin^2 \theta_W$  (19) and it is necessary to solve for consistency. It is worth noting that the corrections described above for the  $W$  and  $Z$  boson mass diagrams also apply to foreground fermion/weak boson interaction vertices. However, note that for the  $Z$  boson, the magnitude of the corrections show some variation between different species, with (for example) the electrons attracting EM loop corrections which are not present for the neutrino. The value obtained for the weak mixing angle will consequently depend on the different weightings given to the various species which may be involved, and thus on the details of individual experiments to measure this parameter. For this reason, the present paper concentrates on particle mass rather than seeking to reproduce experimentally determined values of  $\sin^2 \theta_W$ .

### D. Gluon masses

By the unbroken  $GL(3, \mathbb{R})$  symmetry of the colour sector, in the  $e_{ij}$  basis all gluons have identical mass, and it suffices to calculate the mass of one off-diagonal gluon.

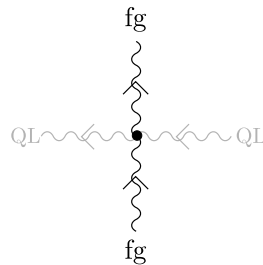


FIG. 5. As the gluon interaction with the QL gluon field need not conserve colour on a per-interaction basis, foreground gluons may interact with a pair of gluons having non-complementary charges.

Evaluation of the gluon mass is therefore similar to evaluation of  $W$  boson mass, and indeed evaluation of the leading order diagram and preon-to-preon gluon loop corrections proceed equivalently. Where the  $W$  and gluon mass calculations diverge is in the contribution from interactions with the QL boson fields. For the  $W$  boson this contribution arose from the QL photon and scalar boson fields. For the gluons, there are couplings to the QL gluon and scalar boson fields.

To evaluate the gluon contribution to the  $\mathcal{O}\{[\mathcal{E}_{\text{QL}}^{(2)}/\mathcal{E}_{\text{QL}}^{(1)}]^2\}$  term, recognise that the preservation of colour cycle invariance across the entirety of  $\mathbb{R}^{0|18}$  dust gravity guarantees that all gluons always appear in the context of a superposition of all nine possible species. Interactions with the QL need not therefore conserve colour charge on an individual gluon on a term-by-term basis provided colour charge is collectively conserved across the superposition. (Individual gluon colour will, however, be preserved on average over length or time scales sufficiently large compared with  $\mathcal{L}_{\text{QL}}$  as the QL has net trivial colour.) For mass interactions, the consequence of this is that rather than interacting with a single looped boson as per Fig. 1(i), a gluon can interact with a pair of different gluons from the QL as per Fig. 5. To evaluate the QL gluon contribution, note:

- This interaction has coefficient  $f^2$ , compared with  $f^2/2$  for the photon.
- A diagram in which the two QL gluons have different field operators on the vertex,  $\varphi^{c_1 \dot{c}_1} \varphi^{c_2 \dot{c}_2}$ , receives a factor of  $\frac{1}{2}$  relative to the photon term due to loss of vertex symmetry, but a factor of two as these fields may be pulled down from the action  $Z$  in either order. A diagram in which the two QL gluons have the same field operator attracts neither of these factors.
- Regardless of how the vertex operators are pulled from  $Z$ , each QL boson independently ranges over all nine possible species for a factor of 81.

The net contribution to gluon mass from the QL gluon field is therefore 81 times larger than the contribution to  $W$  boson mass from the QL photon field. To the same

order as used in Eq. (29) above, the QL gluon mass is therefore given by

$$m_c^2 = 18f^2 \left[ \mathcal{E}_{\text{QL}}^{(1)} \right]^2 \left[ 1 + \left( 64 + \frac{3}{2\pi} - f_Z \right) \frac{\alpha}{2\pi} + O(\alpha^2) \right] \times \left\{ 1 + \frac{99m_e^2}{[k_1^{(e)}]^4 m_W^2} [1 + O(\alpha)] \right\}. \quad (39)$$

As noted in Ref. 1, this is a bare mass and will be corrected by self-interaction terms at energy scales small compared with the strong nuclear force.

With regards to the universality coupling, the gluons have nontrivial representation on  $SU(3)_C$  and thus this coupling must also be evaluated in the  $SU(3)_C$  sector. However, all gluons already couple to all QL boson members of this sector, and thus there are no missing couplings to be recovered using this technique. Any attempt to do so would result in double counting, so no further terms are acquired.

In terms of standard error, and assuming  $O(\alpha^2)$  terms are equivalent for  $W$  bosons and gluons, the most significant effect arising from the next order of corrections beyond those considered is a contribution to  $m_Z$  at approximately  $10^{-1} \sigma_{\text{exp}}$ , while the largest relative contribution is to  $m_W$ ,  $m_Z$ , and  $m_{H'}$ , and is of approximate order of parts in  $10^7$ .

### E. Scalar boson mass

As with the  $W$  and  $Z$  bosons and the gluon, some higher-order corrections to gluon mass are computed here. However, for purposes of this paper it suffices to evaluate only the  $O(\alpha)$  loop terms and ignore the coupling with the QL scalar boson field as this is not relevant to the numerical results presented at the level of precision employed in this paper.

For convenience, as in Ref. 1 the subleading term in the scalar boson mass interaction [Fig. 6(ii), l.h.s.] will be rewritten as a correction to the leading term [Fig. 6(i)], associated with a factor of  $(2\pi)^{-1}$ .

#### 1. Vector boson loops

To evaluate the gluon loop corrections, recognise that the four preons and two antipreons (or vice versa) of the QL in Fig. 6(i) and the r.h.s. of Fig. 6(ii) may be grouped into a QL composite scalar boson and two QL composite vector bosons, with the latter then being mapped into true vector bosons and a numerical scaling factor. The preons may be grouped together in any valid combination which yields these three effective QL particles, with the four preons contributing a factor of  $\binom{4}{2} \binom{2}{1} \binom{1}{1}$  and the two antipreons contributing  $\binom{2}{1} \binom{1}{1}$  for a net factor of 24. However, two of the preons are the same colour, dividing

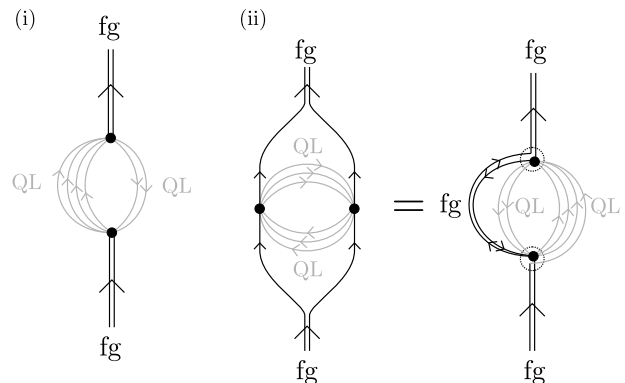


FIG. 6. (i) Leading diagram contributing to scalar boson mass. (ii) First correction.

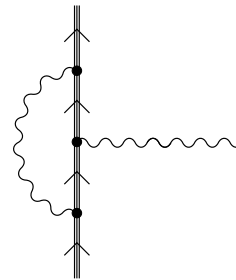


FIG. 7. First-order electromagnetic correction to lepton magnetic moment.

the number of colour-distinct combinations by two (and by construction from fermion channels, these preons also carry the same  $a$ -charge—see Ref. 1, Sec. III F 4), and the two composite vector bosons are functionally equivalent, again reducing the number of distinguishable arrangements by a factor of two, for an overall net factor of 6 from colour arrangements.

Given a particular arrangement of participating preons, it is convenient to work with composite scalar and vector bosons so that each composite particle then admits a gluon loop correction between its two components. However, the loop factor arising from the composite scalar boson is of the opposite sign to those arising from the composite vector bosons as the antipreon is replaced by a second preon, giving a factor of  $-1$ . Other than that, all calculations proceed equivalently.

For a gluon which is diagonal in the  $e_{ij}$  basis, the calculation is directly analogous to the electromagnetic loop correction to magnetic moment (Fig. 7), save that the vertex factors are  $f^2$  not  $f^2/2$ . The contributions from the off-diagonal gluons are necessarily the same by  $GL(3, \mathbb{R})$  symmetry.

Summing these terms therefore yields a net weight for the gluon loop corrections of

$$\frac{12\alpha}{2\pi}. \quad (40)$$

There are no contributions from electroweak boson loops

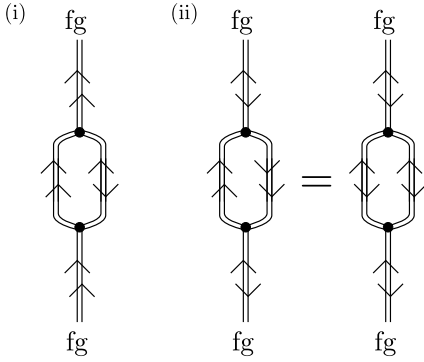


FIG. 8. Scalar boson corrections to the species appearing within the scalar boson mass vertex: (i) When a scalar boson loop correction is added to the scalar boson propagator, this replaces one preon in the original propagator with its antiparticle, resulting in a sum over composite vector bosons. The resulting diagram is then identical to that obtained when vector boson loop corrections are applied to the scalar boson propagator. These diagrams have also already been counted. (ii) The scalar boson loop correction to a composite vector boson propagator yields an internal loop comprising two scalar bosons. Swapping the sides of this internal loop reveals equivalency to a sum over composite vector boson corrections to the composite vector boson propagator, and these can be rewritten as fundamental vector boson corrections to the composite vector boson propagator. These diagrams have also already been counted.

as the  $H'$  boson carries no net electroweak charges, so this is the total contribution from vector boson loops.

## 2. Scalar boson loops

Now consider scalar boson loop corrections to the scalar boson mass term. Once again, these act on the effective composite vector and scalar bosons connecting the mass interaction vertices. However, recalling that a scalar boson interaction vertex always maps one connected preon into its antiparticle, this always results in a change of particle species within the loop. The interaction between the looping species and the QL preon fields is inserted explicitly in one arm of the loop, but is also implicitly present in the other arm of the loop as the other particle is also taken to be massive. Thus the explicit QL preon interaction may be freely moved from one arm to the other. Therefore, first consider the diagrams into which these interaction vertices will be inserted:

- The scalar boson loop correction to the scalar boson propagator has an internal loop comprising one scalar boson and one composite vector boson. The composite vector boson may be mapped into a fundamental vector boson and a numerical factor using Eqs. (80–81) of Ref. 1. The factor cancels with that arising from the construction of  $H'H'^*$ . Freedom to insert the explicit QL coupling in either

limb of the loop yields that the scalar boson correction to the scalar boson propagator is exactly equivalent to a sum over vector boson loop corrections to the scalar boson propagator. They must not be counted twice.

- The scalar boson loop correction to the composite vector boson propagator has an internal loop comprising two scalar bosons. As in Sec. II A 1 c this may be evaluated by rearranging the internal preon lines. However, on doing so, it is immediately seen to be equivalent to a vector boson loop correction to the composite vector boson field and thus also has already been counted.

For a propagating scalar boson, there are therefore no independent scalar boson loop corrections at  $O(\alpha)$ , and the net expression for scalar boson mass incorporating all boson loop corrections is

$$m_{H'}^2 = 40f^2 \left[ \mathcal{E}_{\text{QL}}^{(1)} \right]^2 \left( 1 + \frac{1}{2\pi} \right) \times \left( 1 + \frac{6\alpha}{\pi} + O \left\{ \left[ \frac{\mathcal{E}_{\text{QL}}^{(2)}}{\mathcal{E}_{\text{QL}}^{(1)}} \right]^2 \right\} + O(\alpha^2) \right). \quad (41)$$

In terms of standard error, the most significant effect arising from the next order of corrections beyond those considered is a contribution to  $m_{H'}$  at approximately  $10^{-1} \sigma_{\text{exp}}$ , while the largest relative contribution is to  $m_{H'}$ , to approximate order of parts in  $10^5$ .

## F. Neutral boson gravitation

One final note regarding the universality coupling described in Secs. II B 2 b and II B 2 b. Although the  $Z$  boson is uncharged, through this process it acquires a means of coupling to the photon *pair* field and thus engaging in the gravity-equivalent interaction of Ref. 1, Sec. III G 3.

The foreground gluons (including the vector dilaton gradient) couple to the colour charges on both the QL preon and gluon fields, and application of the universality coupling allows the QL preon fields to be reduced to composite vector bosons in 1:1 correspondence with the gluons, so the composite to fundamental boson duality does not reveal any new couplings. However, the inclusion of all possible colour couplings implies that a subset of the composite vector boson fields may also be rewritten to correspond to the two-photon coupling (carrying the photon  $a$ -charge, and being summed over all possible neutral colour combinations). As this coupling is constructed from the same composite vector boson fields already accounted for, it makes no additional contribution to inertial mass. However, as it is a coupling to the photon pair field it does grant gravitational mass to the nine gluon fields. Most notably, this interaction imparts gravitational mass to the neutral gluon, or vector dilaton gradient (which is an axion-like particle). This is therefore a potential dark matter candidate.

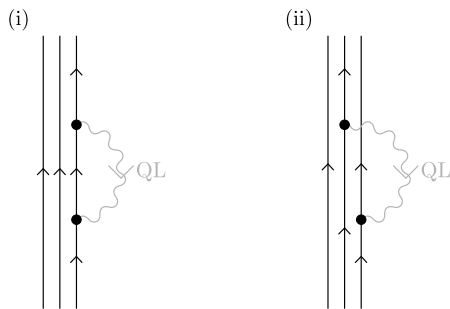


FIG. 9. The fundamental interaction giving rise to lepton mass: The triplet of preons scatters twice off the bosonic component of the background quantum liquid. Either (i) the same, or (ii) different preons may be involved on each occasion, with the upper and lower vertices independently each connecting to any of the three preons. This results in a total of nine diagrams, three having the form of diagram (i) and six having the form of diagram (ii). These nine diagrams are then summed.

### III. LEPTON MASS INTERACTION

#### A. Leading order

The fundamental interaction giving rise to lepton mass is a double scattering of the preon triplet off the vector boson component of the QL (Fig. 9). Both of these diagrams may be considered mean field theory expansions of a loop correction to the fermion propagator in the presence of the QL, but it is more convenient to refer to these as “leading order” diagrams, and to count the number of (foreground) loop corrections to these leading order diagrams, e.g. 1-loop corrections to the leading order diagram, etc. Henceforth such corrections will be termed simply “1-loop corrections”.

Figure 9 is constructed by generating a pair of interaction vertices between the lepton and both the  $SU(9)$ -valued gauge boson field (representation  $\mathbf{80}$ ) and the dilaton gradient field (trivial representation,  $\mathbf{1}$ ). These representations are then factorised according to

$$\begin{aligned} SU(9) \oplus \mathbf{1} &\cong [SU(3)_A \oplus \mathbf{1}_A] \otimes [SU(3)_C \oplus \mathbf{1}_C] \\ \mathbf{80} + \mathbf{1} &= (\mathbf{8} + \mathbf{1}) \times (\mathbf{8} + \mathbf{1}) \end{aligned} \quad (42)$$

where each instance of  $\mathbf{1}$  represents the appropriate trivial representation. Finally, each  $SU(3)$ -valued boson field is expanded in terms of its components, and terms are discarded where the mean magnitude-squared of the QL component of the boson field vanishes by gauge. The resulting interactions may each involve any of the three preons making up the lepton. As per Eqs. (1–2) and (11), the bosons may be

- the photon, associated with the 1-dimensional rep-

resentation of  $SU(3)_C$  whose generator is

$$\lambda_9 = \frac{1}{\sqrt{3}} \begin{pmatrix} 1 & 0 & 0 \\ 0 & 1 & 0 \\ 0 & 0 & 1 \end{pmatrix}, \quad (43)$$

- gluons, associated with the 8-dimensional representation  $\{\lambda_i | i \in \{1, \dots, 8\}\}$  of  $SU(3)_C$  generated by the rescaled Gell-Mann matrices (A3), or
- the vector dilaton, also associated with  $\lambda_9$ .

By Eq. (3), the separation of the two boson source/sinks is of order  $\mathcal{L}_{QL}$ .

To evaluate the contribution of the QL fields to lepton mass, it is helpful to separate the consequences of these boson interactions into two parts. First, there is the action of the representation matrices of  $SU(3)_C$  on the preon fields, and second, there is the numerical mass term arising from the mean square value of the QL boson field. As noted in the introduction, the family of gluons will be taken to include the vector dilaton gradient, giving a combined symmetry group

$$SU(3)_C \oplus \mathbf{1} \cong GL(3, \mathbb{R})_C. \quad (12)$$

It is then helpful to note that this 9-membered family admits representation both in terms of the Gell-Mann and identity matrices (basis  $\{\lambda_i | i \in \{1, \dots, 9\}\}$ ) and in terms of the elementary matrices  $\{e_{ij} | i \in \{1, 2, 3\}, j \in \{1, 2, 3\}\}$ .

#### 1. Action on colour sector

To begin with the action of the generators of  $GL(3, \mathbb{R})_C$ , note that over the course of a propagator of length  $\mathcal{L} \gg \mathcal{L}_{QL}$ , a lepton will engage in a near-arbitrarily large number of interactions with the background QL fields. Each interaction will apply a  $gl(3, \mathbb{R})$  representation matrix from  $\{\lambda_i | i \in 1, \dots, 9\}$  depending on the boson species with which the lepton interacts. In the absence of foreground  $W$  or  $Z$  bosons, the QL is made up entirely of photons and gluons.

Given a preon of colour  $c_1$ , this may have nonvanishing interaction with the photon or any of three gluons in the elementary basis  $e_{ij}$ . For example, if  $c_1 = r$  then admissible gluons are  $c^{rr}$ ,  $c^{gr}$ , and  $c^{br}$ . Heuristically, their action on the colour space may be represented as

$$c^{rr}|r\rangle \rightarrow |r\rangle \quad c^{gr}|r\rangle \rightarrow |g\rangle \quad c^{br}|r\rangle \rightarrow |b\rangle \quad (44)$$

where all associated numerical factors have been ignored for illustrative purposes.

More generally, the family of gluons acts on a vector of preon colours as indicated by

$$\begin{pmatrix} c^{rr} & c^{rg} & c^{rb} \\ c^{gr} & c^{gg} & c^{gb} \\ c^{br} & c^{bg} & c^{bb} \end{pmatrix} \begin{pmatrix} |r\rangle \\ |g\rangle \\ |b\rangle \end{pmatrix}. \quad (45)$$

It is worth noting that there is no emergence of colour superselection for individual particles in  $\mathbb{R}^{0|18}$  dust gravity, as the  $\text{GL}(3, \mathbb{R})_C$  symmetry is unbroken, so there exists a freedom of basis on the colour sector corresponding to an arbitrary global transformation in  $\text{SU}(3)_C$ . Any coloured fundamental or composite particle may be put into an arbitrary superposition of colours using such a transformation, though relative colour charges of different particles remain unchanged, as does the magnitude of the overall colour charge of a composite particle.

Recognise now that Fig. 9 contains contributions to two mass vertices. Although their contributions to fermion mass are nonvanishing only when they appear pairwise, as shown in Fig. 9, there is no requirement for this pair to be consecutive. It suffices that each vertex be paired with a conjugate vertex separated by distance and time no greater than  $\mathcal{L}_{\text{QL}}$  (which is within a few orders of magnitude of Planck length) in the isotropy frame of the QL. Indeed, these vertices are connected by a foreground fermion propagator which in general also undergoes further interactions with the QL, represented by using a massive propagator for this fermion and requiring consistency with the outcome of the mass vertex calculation. In general a foreground fermion exhibiting a net propagation over distance or time of  $\mathcal{O}(\mathcal{L}_{\text{QL}})$  in the isotropy frame of the QL will scatter back and forth multiple times in this process, interacting with  $\mathcal{O}(\langle N_{\text{QL}} \rangle) \sim 10^{36}$  particles from the QL, and consequently the number of unpaired vertices is negligible. Furthermore, where unpaired vertices do exist, their net effect vanishes on average over length or time scales larger than  $\mathcal{L}_{\text{QL}}$ . It is therefore reasonable to assume during evaluation that each vertex belongs to a pair.

Counting vertices arising from Fig. 9, for every photon vertex there is also on average one vertex for each of the nine gluons. Across macroscopic length scales, deviations from this average relative frequency will be negligible.

Consider now the specific case of interactions between a propagating lepton and the bosons of the QL. Each preon may interact either with a photon or with any of the nine gluons, and the action of the photon on the space of preon colours is trivial, so it is convenient to ignore the photon for now and reintroduce it later.

As already noted, paired interactions with the QL gluon field conserve the net colour-neutrality of a leptonic preon triplet. However, overlapping and intercalation of multiple interaction pairs implies that this property only holds on average, as any colour measurement will interrupt a finite number of mass interactions and thus summation to yield no net colour charge on the preon triplet cannot be assured. It is desirable that any measurement of lepton colour should be null, not just the average, and thus a local change of co-ordinates on  $\text{SU}(3)_C$  must be performed on a co-ordinate patch encompassing the non-interacting preons such that changes in their colours track those of the interacting preon. This change of co-ordinates is not part of the choice of gauge on  $\text{SU}(3)_C$ , and thus is in principle associated with construction of

some synthetic boson interactions where it intersects with particle worldlines. As described in Sec. III F 2 of [1], the vertex factors associated with these interactions arise from the representation matrices of  $\text{SU}(3)_C$  given as  $\lambda_i$  in Appendix A. By construction these bosons are constrained to have no effect beyond the colour shifts associated with the boundary of the patch, and to leading order this effect is parameterless. In the leading order diagram these bosons consequently have no degrees of freedom, carry no momentum, and thus may be integrated out to yield a factor of 1. Consequently they are not drawn. Only the factors arising from the representation matrices persist, acting on the colour vector of an individual preon as the matrix

$$K_\ell = \begin{pmatrix} 1 & A & A^\dagger \\ A^\dagger & 1 & A \\ A & A^\dagger & 1 \end{pmatrix}, \quad A = \pm \frac{1 \pm i}{2}. \quad (46)$$

The sign on  $i$  is free to be chosen by convention, while the overall sign on  $A$  is fixed by noting that cyclic permutation of colours, which is in  $(K_\ell)^3$ , is required to leave the sign of an eigenstate of  $K_\ell$  unchanged. The eigenvalues of  $K_\ell$  must therefore be non-negative, setting

$$A = -\frac{1 \pm i}{2}. \quad (47)$$

Choosing a sign for  $i$ , the mixing matrix  $K_\ell$  may then be written

$$K_\ell(\theta_\ell) = \begin{pmatrix} 1 & \frac{e^{i\theta_\ell}}{\sqrt{2}} & \frac{e^{-i\theta_\ell}}{\sqrt{2}} \\ \frac{e^{-i\theta_\ell}}{\sqrt{2}} & 1 & \frac{e^{i\theta_\ell}}{\sqrt{2}} \\ \frac{e^{i\theta_\ell}}{\sqrt{2}} & \frac{e^{-i\theta_\ell}}{\sqrt{2}} & 1 \end{pmatrix} \quad \theta_\ell = -\frac{3\pi}{4}. \quad (48)$$

As noted in Ref. 1, Sec. III F 2, this matrix bears a strong resemblance to Koide's  $K$  matrix for leptons [3]. The minus sign on Koide's off-diagonal component  $S(\theta_f)$  has been absorbed into the phase  $\theta_\ell$ , and the free parameters  $a_f$ ,  $b_f$ , and  $\theta_f$  are fixed by the geometry of the model, in keeping with the predictive capacity of  $\mathbb{R}^{0|18}$  dust gravity.

Recognising that on average all QL gluons act identically and with equal frequency, it is convenient to collect these together into a single  $\text{gl}(3, \mathbb{R})$ -valued gluon associated with two applications of matrix  $K_\ell$  to the non-interacting preons, as shown in Fig. 10.

Now recognise that since the gluons of  $\mathbb{R}^{0|18}$  dust gravity are massive, and since the fundamental mass interactions take the form of loop diagrams with respect to the lepton propagator (Fig. 9), these will be suppressed by a factor of  $\mathcal{O}(m_\ell^2/m_c^2)$  relative to the photon contribution. With each gluon interacting, on average, once for every photon interaction, it is convenient to write the direct contributions of the gluon terms to particle mass as corrections to the larger photon term and to associate copies of the matrix  $K_\ell$  with the photon vertices in a manner equivalent to that shown in Fig. 10.

Next, consider that the preons on which matrix  $K_\ell$  are acting are just two of three preons in a colour-neutral

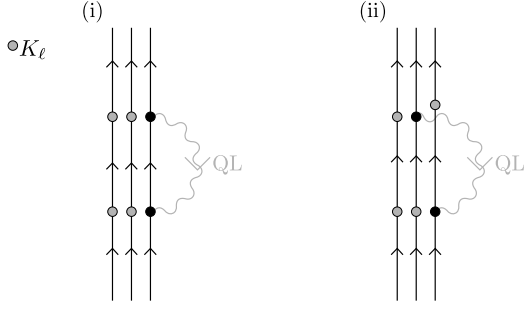


FIG. 10. When a composite fermion interacts with the gluons from the QL, represented as a single  $\mathfrak{gl}(3, \mathbb{R})$ -valued boson, the colour mixing process represented by matrix  $K_\ell$  acts on all preons not coupling to the boson at any given vertex. Diagrams (i) and (ii) correspond to Figs. 9(i)-(ii) respectively. Once again these are just two representative diagrams from a family of nine, as the upper and lower vertices may independently each be connected to any of the three preons. This results in a total of nine diagrams, three having the form of diagram (i) and six having the form of diagram (ii).

triplet. For leptons, all three  $a$ -charges are identical and thus over macroscopic scales, where chance fluctuations become negligible, matrix  $K_\ell$  will act identically on each member of the triplet. This symmetry is convenient, as it allows the study of an individual preon prior to the reconstruction of the triplet as a whole.

As per Eq. (5), the preons making up observable leptons are now eigenstates of this matrix  $K_\ell$ , corresponding to the eigenvectors

$$v_1 = \frac{1}{\sqrt{3}} \begin{pmatrix} 1 \\ 1 \\ 1 \end{pmatrix} \quad (49)$$

$$v_2 = \frac{1}{\sqrt{3}} \begin{pmatrix} e^{\frac{\pi i}{3}} \\ e^{-\frac{\pi i}{3}} \\ -1 \end{pmatrix} \quad (50)$$

$$v_3 = \frac{1}{\sqrt{3}} \begin{pmatrix} e^{\frac{2\pi i}{3}} \\ e^{-\frac{2\pi i}{3}} \\ 1 \end{pmatrix} \quad (51)$$

which are independent of  $\theta_\ell$  and have eigenvalues  $\{k_i^{(\ell)} | i \in \{1, 2, 3\}\}$  given by

$$k_n^{(\ell)} = 1 + \sqrt{2} \cos \left( \theta_\ell - \frac{2\pi(n-1)}{3} \right). \quad (52)$$

To reconstruct the lepton as a whole, recognise that for three preons at  $\{x_i | i \in \{1, 2, 3\}\}$ , with corresponding colours  $c_i$ , and with the preon at  $x_1$  having a well-defined color, say  $c_1 = r$ , colour neutrality and colour cycle invariance imply that a choice  $c_2 = g$ ,  $c_3 = b$  is equal up to a sign to the alternative choice  $c_2 = b$ ,  $c_3 = g$  (as this exchange corresponds to spatial exchange of two fermions), and thus it suffices to consider only one such colour assignment (say  $c_2 = g$ ,  $c_3 = b$ ) along with spatial permutations. Putting preon 1 into a superposition of colour

states then corresponds to a superposition of cyclic spatial rearrangements of the members of the triplet, with colours  $c_1 = r$ ,  $c_1 = g$ , and  $c_1 = b$  corresponding to colour assignments *with respect to spatial co-ordinate  $x$*  of  $rgb$ ,  $gbr$ , and  $brg$  respectively. It follows that for leptons, colour superselection need *not* be violated, and instead the different spatial configurations of colours on the preon triplet are eigenvectors of a matrix  $K_\ell^{(3)}$  with eigenvalues identical to those of  $K_\ell$ . It appears unlikely that a similar recovery of colour superselection can be achieved for the quarks.

Having established through colour cycle invariance that the matrix  $K_\ell$  acts identically on all constituents of a lepton, and through Fig. 10 that two copies of  $K_\ell$  act per QL photon interaction, it follows that the effect of matrix  $K_\ell$  is to contribute a factor of  $[k_i^{(\ell)}]^2$  to the mass of a lepton of generation  $i$ . It might seem problematic that for  $\theta_\ell = -3\pi/4$ ,  $k_1^{(\ell)} = 0$ , but it will be seen in Sec. III C that  $\theta_\ell$  acquires corrections from higher-order diagrams, resulting in  $k_i > 0 \forall i$ , so  $k_1^{(\ell)}$  may be assumed real and positive, and this concern may be disregarded.

## 2. Mass from photon and gluon components of QL

The zeroth-order electromagnetic term is readily evaluated by making a mean-field substitution (1) for  $[A^\mu(x)A_\mu(y)]_{\text{QL}}$ . For a charged lepton  $\ell_i$  of generation  $i$ , this initial approximation may be written

$$m_{\ell_i}^2 = f^2 [k_i^{(\ell)}]^4 [\mathcal{E}_{\text{QL}}^{(2)}]^2. \quad (53)$$

Note that there is a symmetry factor of two corresponding to exchange of the two QL interactions. This may be understood in either of two related ways:

1. For diagrams such as Fig. 9 which separate into two separate terms on performing the mean field expansion of the QL, one approach is to recognise that each term corresponds to a mass vertex and has its external legs truncated independently. These two vertices are then indistinguishable.
2. Alternatively, for any diagram, including ones which do not separate, recognise that the mass-squared is always applied in the context of an untruncated fermion propagator, say from  $x$  to  $y$ . In this context, all fermion connections to the interaction vertices are again untruncated. (Optionally, the full expression for propagation from  $x$  to  $y$  is then used to infer an equivalent mass term, and the diagram may then be replaced by one in which this mass term is inserted into the propagator twice.) Applying either form of this approach to Fig. 9, the diagram for propagation between two points is again seen to attract a symmetry factor of two.

Now consider interactions between a foreground fermion and the QL gluon fields. As with the photon,

these interactions take the form of loop diagrams evaluated in the mean-field regime for the QL, and as noted in Ref. 1, the fermion may transiently surrender momentum to or borrow momentum from the QL. However, in contrast with the photon loop evaluated to obtain Eq. (53), the gluon field is massive, and when a foreground particle transfers momentum to a gluon field, this results in an effective foreground excitation of that gluon field. Foreground excitations acquire mass, and thus both limbs of the loop must be considered massive. However, the separation of the two vertices is of  $O(\mathcal{L}_{\text{QL}})$ , which is much shorter than the strong interaction scale, so the gluon exhibits only its bare mass (39). This gives rise to a loop-associated factor of  $m_\ell^2/m_c^2$ . This factor vanishes for the photon, as it is massless, but not for interactions with the QL gluon field.

In both cases, evaluation of momentum flux around the loop may be taken to yield a factor of

$$\frac{\alpha}{2\pi} \mathbf{f} \left( \frac{m_\ell^2}{m_b^2} \right), \quad b \in \{A, c\} \quad (54)$$

where  $\mathbf{f}(n) \rightarrow 1$  as  $n \rightarrow \infty$ . For the photon the factor of  $\alpha/(2\pi)$  is absorbed into the QL mean-field term by definition, and factor  $\mathbf{f}(\cdot)$  reduces to 1. For gluons, dependence on the same energy scale  $\mathcal{E}_{\text{QL}}^{(2)}$  indicates that an identical factor of  $\alpha/(2\pi)$  is absorbed into the mean field term, while the mass dependence of  $\mathbf{f}(\cdot)$  reveals that the gluon terms are suppressed by a factor of  $m_\ell^2/m_c^2$  relative to the photon term.

Working in the  $e_{ij}$  basis, consider first an off-diagonal gluon. When this gluon is emitted, it changes the colour of the emitting preon. For example, the colours of the preon triplet may change from  $rgb$  to  $rgg$ . However, a mass vertex must by definition leave the fermion on which it acts unchanged, and thus to generate a mass term the gluon must be absorbed by the same preon as it was emitted, restoring the original state ( $rgb$ ). Absorption by a different preon is a valid physical process, but instead comprises part of the binding interaction between the preons. This is in contrast to the photon, where emission and absorption may be on different preons without affecting either the  $a$ -charge or the  $c$ -charge configuration.

Overall, expressed relative to the photon interaction, factors for an off-diagonal gluon arise as follows:

- A given gluon may only be emitted by a preon of specific colour, for a relative factor of  $\frac{1}{3}$ .
- However, any of the three preons may be this colour, for a relative factor of three.
- The photon may be absorbed by any of the three preons, whereas each gluon may be absorbed only by the preon which emitted it, for a relative factor of  $\frac{1}{3}$ .
- Vertices are associated with factors of  $f$ , not  $f/\sqrt{2}$ , for a relative factor of two.

- Vertices are no longer interchangeable, for a relative factor of  $\frac{1}{2}$ .
- Interactions between a fermion and an off-diagonal boson attract a structural factor of  $\frac{5}{3}$ . (For a comparable calculation see the  $W$  correction to the EM vertex [2], in which the arising factor of  $\frac{10}{3}$  comprises a factor of 2 from the change in vertex factor and a structural factor of  $\frac{5}{3}$ .)
- As previously noted, there is a mass factor of  $m_\ell^2/m_c^2$ .

By  $\text{GL}(3, \mathbb{R})$  symmetry, each of the nine gluons will yield the same magnitude contribution to fermion mass, for a further factor of nine. Taking both photon and gluon terms into account, the leading-order expression for photon and gluon contribution to lepton mass is therefore given by

$$m_{\ell_i}^2 = f^2 [k_i^{(\ell)}]^4 [\mathcal{E}_{\text{QL}}^{(2)}]^2 \left( \frac{q_\ell^2}{e^2} + \frac{5m_{\ell_i}^2}{m_c^2} \right) \quad (55)$$

where  $q_\ell$  is the charge of lepton  $\ell_i$ .

As an aside, for the fermions there is no equivalent to the bosonic universality coupling explored in Sec. II B 2 b. For the  $Z$  boson, this coupling arises as the basic  $Z$  mass diagram [equivalent to Fig. 1(i)] intrinsically incorporates six QL preon lines, and two co-ordinates to integrate over, permitting reduction to two preon lines when one of these integrals is performed. In contrast, the basic fermion mass diagram (Fig. 10) contains no intrinsic mechanism for adding extra preon lines. Although extra preons may be recruited from the QL, consistent normalisation [1, Sec. III F 1] requires that integrating over the additional co-ordinate thus introduced will inevitably eliminate them again.

### 3. Mass from scalar component of QL

Next to be considered is the interaction between the composite lepton and the QL composite scalar boson field. Again it is desirable to write this term as a correction to the photon term.

To achieve this, recognise that the scalar boson is made up of a sum over nine components. Likewise, when the  $\text{SU}(3)_A$  sector is supplemented by the vector dilaton gradient this results in a symmetry group  $\text{GL}(3, \mathbb{R})_A$  whose Lie algebra  $\mathfrak{gl}(3, \mathbb{R})_A$  also has nine elements. The interaction vertex for each component of the scalar boson may be obtained by transforming that of a boson from  $\mathfrak{gl}(3, \mathbb{R})_A$  associated with basis element  $e_{ij}$ . There are nine such bosons, which include the  $W$  and  $W^\dagger$  bosons. Note that the boson gauges [1, (127–131)] do not impact the fermion sector, and the scalar boson is constructed from two fermionic preons, so all nine terms must be taken into account regardless of whether the associated

boson is eliminated by gauge, and since the symmetry of the fermion sector is unbroken, all nine terms are equal.

Note that although the numerical factors associated with the scalar boson correction is obtained by transforming the equivalent vector boson corrections, this is not double counting because the scalar boson involved is a foreground particle, and therefore massive, with a mass shell distinct from that of the numerically convenient bosons. This is in contrast with Sec. II E 2, where all involved particles are effectively massless and thus a numerical identification corresponds with a physical identification.

By the internal  $GL(3, \mathbb{R})$  symmetry of the scalar boson, all terms contribute equally to the fermion/scalar boson interaction. Considering the off-diagonal term corresponding to  $W$ , the following factors arise:

- Relative to the photon, the  $W$  boson interaction acquires a structural factor of  $\frac{5}{3}$ .
- Relative to the photon, the  $W$  boson coupling is stronger by a factor of two.
- Compared with the photon, there is a loss of vertex interchangeability for a factor of  $\frac{1}{2}$ . (Recall that external legs are not truncated so vertices in Fig. 9 are not distinguishable.)
- However, this is offset by a factor of two corresponding to the different ways to attach the external source and sink to the now-distinguishable vertices.
- Transforming a  $WW^\dagger$  pair into a term in the  $H'H'^*$  pair [in principle performed using Eqs. (80–81) of Ref. 1 and integration by parts] yields one of nine terms in  $H'H'^*$ , so introduces a factor of  $-\frac{2}{9} [\mathcal{E}_{QL}^{(2)}/\mathcal{E}_{QL}^{(1)}]^2$  from Eqs. (4) and (6).
- The scalar boson contributes an internal symmetry factor of two relating to crossing or not crossing its internal preon lines.
- There is no factor of  $[1 + 1/(2\pi)]$  for this interaction, as there is only one relevant type of vertex interaction involving the scalar boson field and the fermion field. This may be contrasted with Fig. 6, where there are two relevant types of vertex [seen in diagrams (i) and (ii) respectively] with each having different couplings to the preonic constituents of the scalar boson.
- Related to the above, twisting the inner preon line to yield an additional loop particle as shown in Fig. 12 changes the scalar boson loop correction into a composite vector boson loop correction. However, in contrast with the vector boson loops in Sec. II A 1 (and by similar argument the composite vector bosons appearing in Sec. II E) this loop is not constrained to vanish at large scales greater than

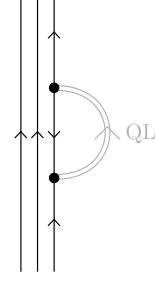


FIG. 11. Leading-order contribution to fermion mass from the  $QL$  scalar field.

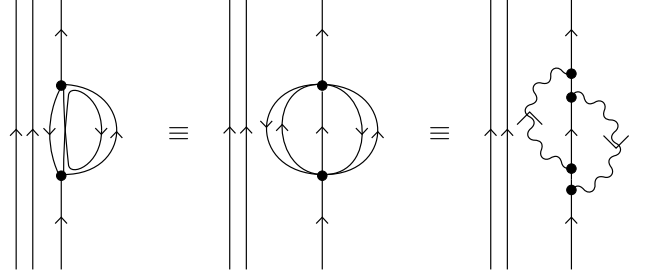


FIG. 12. Twisting the inner preon line to yield an additional loop particle changes the scalar boson loop correction into a composite vector boson loop correction. As the loop is foreground, with dominant contribution from massive trajectories traversing length scales large compared with  $\mathcal{L}_{QL}^{(2)}$ , it must be re-expressed in terms of fundamental vector bosons.

$\mathcal{L}_{QL}^{(1)}$ . As observed in Sec. III D 3 of Ref. 1, incorporating both fundamental and composite vector bosons into the particle spectrum of the low-energy ( $\mathcal{L} \gg \mathcal{L}_{QL}$ ) regime is redundant and therefore the composite vector bosons must be re-expressed as fundamental vector bosons. The resulting diagram involves two boson loop corrections, and is not a scalar loop term at all. Similarly, twisting twice restores a scalar boson, but once again yields a redundant representation of vector boson loops, which are higher-order terms in the correction series.

There are nine bosons in the  $e_{ij}$  basis for a final factor of 9. Using lowest-order expressions for  $\mathcal{E}_{QL}^{(1)}$  (14) and  $\mathcal{E}_{QL}^{(2)}$  [1, Eq. (192)] yields a weight relative to the photon term of

$$240 \frac{m_{\ell_i}^2}{m_{H'}^2} \frac{m_{\ell_1}^2}{[k_1^{(\ell)}]^4 m_W^2} [1 + O(\alpha)] \quad (56)$$

for a total lepton mass

$$m_{\ell_i}^2 = f^2 [k_i^{(\ell)}]^4 [\mathcal{E}_{QL}^{(2)}]^2 \times \left\{ \frac{q_\ell^2}{e^2} + \frac{5m_{\ell_i}^2}{m_c^2} + \frac{240m_{\ell_i}^2 m_{\ell_1}^2}{[k_1^{(\ell)}]^4 m_{H'}^2 m_W^2} \right\}. \quad (57)$$

The most significant contribution from the higher-order correction to Eq. (56) is to  $m_Z$  at  $O(10^{-2}\sigma_{\text{exp}})$  (and in relative terms, to  $m_W$ ,  $m_Z$ , and  $m_{H'}$  to order of parts in  $10^7$ ) so this term may safely be dropped.

#### 4. Gluon and scalar field mass deficits

Conservation of energy/momentum implies that the rest mass imparted to the fermion must be compensated by a reduction in the zeroth component of 4-momentum of some of the QL fields. Likelihood of contribution from any given QL sector will be governed by availability of zeroth-component energy within that sector, i.e. the rest mass of the associated species, and the strength of coupling to that sector. It therefore follows that this borrowing of rest mass occurs with equal likelihood from each of the nine gluon channels of the QL, with much lower likelihood from the scalar boson channel (due to a much weaker coupling), and not at all from the photon channel (due to zero rest mass). For a first approximation, consider only the gluon channel. Borrowing a mass of  $m_*^2$  from a QL gluon field takes place at the first of the existing gluon/fermion interaction vertices of Fig. 9, and corresponds to deletion of a gluon of mass  $m_*$  from the QL. This hole then propagates as a quasiparticle, and is filled by the conjugate interaction at the second vertex.

More generally, with multiple overlapping pairs of QL gluon field interactions occurring along a fermion propagator, there is a consistent propagating hole in the QL gluon sector corresponding to an energy deficit of  $m_*c^2$ , and individual vertices may cause transient fluctuations and may change which specific gluon fields (with respect to some arbitrary choice of colour basis) are involved in propagating this hole, but in general it may be in any of the nine gluon channels at any time. This hole is in addition to the effect discussed in Sec. III A 2 where fermions may surrender momentum to or borrow momentum from the QL, and thus gives an additional correction factor not yet discussed.

This hole propagates as a quasiparticle accompanying the lepton. Any time that a fermion interacts with the QL gluon sector this hole is necessarily also present, and may occupy any of nine channels.

For simplicity, further consider the case when the hole occupies an off-diagonal channel. It would be convenient to write the effect of this hole as a correction to the mass of gluon,

$$m_c^2 \longrightarrow m_c^2 - km_*^2 \quad (58)$$

for some factor  $k$ . Recognising that the co-propagating hole's interaction with the fermion is trivial (it is only required to be present), with any local energy/momentum transfer to or from the QL being mediated by the fermion/gluon coupling of Fig. 9(i), the hole's interactions attract no structural vertex factor and thus where the direct gluon interactions of Fig. 9(i) generate a factor of  $5/(3m_c^2)$ , the hole will contribute only  $-m_*^2$ . Further,

the presence of the hole breaks the time reversal symmetry of a portion of the QL and this gives rise to a symmetry factor of  $\frac{1}{2}$  relative to the original gluon interaction in which the QL was assumed time-reversal-invariant. Finally, there are nine gluon channels, each of which yields an equivalent correction by  $GL(3, \mathbb{R})$  symmetry. The net outcome is to correct the gluon mass to an effective mass of

$$(m_c^*)^2 = m_c^2 \left( 1 - \frac{27 m_*^2}{10 m_c^2} \right). \quad (59)$$

Note that  $m_c^*$  is a function of  $m_*$ , but for a lepton  $\ell_i$  which is on-shell and at (or close to) rest in the isotropy frame of the QL this admits the replacement  $m_*^2 \rightarrow m_{\ell_i}^2$  and can then be conveniently left implicit. Also note that the gluon mass deficit effect is a whole-field effect, acting on both the foreground and QL gluon fields. The corrected gluon mass  $m_c^*$  should be used anywhere a particle interacts with a gluon field in the presence of a lepton. The lepton mass equation is amended to

$$m_{\ell_i}^2 = f^2 \left[ k_i^{(\ell)} \right]^4 \left[ \mathcal{E}_{\text{QL}}^{(2)} \right]^2 \times \left\{ \frac{q_{\ell}^2}{c^2} + \frac{5m_{\ell_i}^2}{(m_c^*)^2} + \frac{240m_{\ell_i}^2 m_{\ell_1}^2}{\left[ k_1^{(\ell)} \right]^4 m_{H'}^2 m_W^2} \right\}. \quad (60)$$

Similarly, the foreground lepton may also borrow its mass from the scalar boson field. However, coupling between leptons and scalar bosons is weaker than that between leptons and gluons, and this correction falls below the threshold of relevance, giving rise primarily to corrections to  $m_Z$  at  $O(10^{-2}\sigma_{\text{exp}})$  (or in relative terms, to  $m_{\tau}$ ,  $m_Z$ ,  $m_W$ , and  $m_{H'}$  to order of parts in  $10^7$ ).

## B. Foreground Loop Corrections

Now consider the effects of foreground loop corrections on the leading-order diagrams of Figs. 9 and 11. Note that since momentum is continually redistributed among the constituent preons by means of gluon-mediated interactions even over length scale  $\mathcal{L}_{\Psi}$ , a boson need not start and finish its trajectory on the same preon in order to be considered a loop correction to an emission vertex. Further note that the massive nature of the loop boson does not disrupt the QL correlators in these diagrams, as these are brought together through the use of spinor identities at the vertices making these diagrams more robust against interference from outside the autocorrelation region than the boson mass diagrams of Sec. II.

### 1. 1-loop EM corrections

The  $O(\alpha)$  EM loop corrections to the lepton mass interaction are shown in Fig. 13. These should be compared

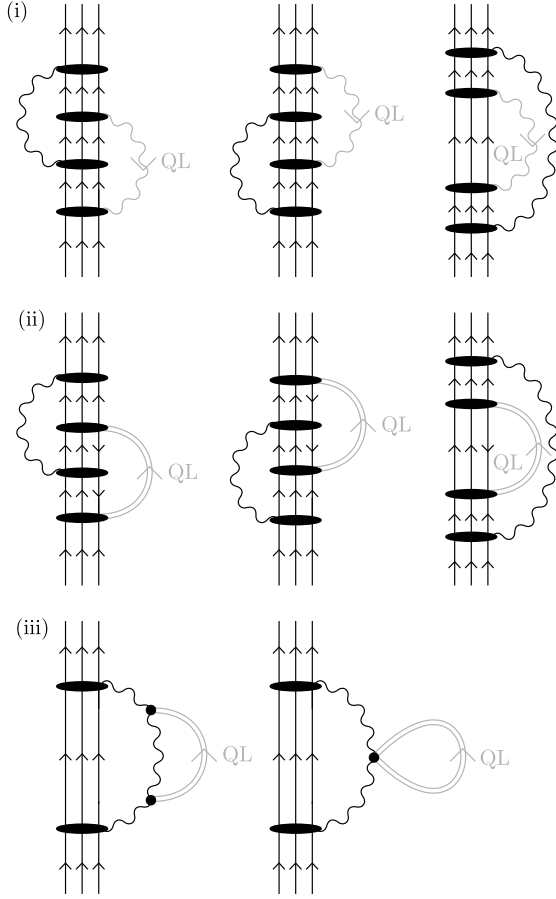


FIG. 13. One-foreground-loop EM corrections to (i) vector boson and (ii)-(iii) scalar boson lepton mass interactions. The broad oval interaction vertices indicate that the boson may interact with any of the three preons, and all configurations should be summed over.

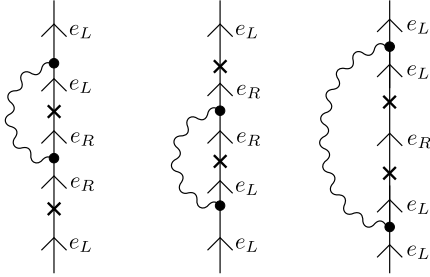


FIG. 14. Standard Model one-foreground-loop EM corrections to the electron mass vertex. The example shown is for the left-helicity electron Weyl spinor; equivalent diagrams for the right-helicity spinor exchange  $L$  and  $R$ .

with their Standard Model counterparts in Fig. 14.

As in Sec. II A 1, the only corrections which need to be incorporated into the electron mass vertex are those which do not also appear in the Standard Model. However, comparing the diagrams of Fig. 13(i) with their counterparts in Fig. 14 reveal these to be directly equivalent. The diagrams of Fig. 13(i) are therefore accounted

for in the usual Standard Model corrections, making no contribution to  $m_{\ell_i}$ .

Next, consider the scalar boson loops of Fig. 13(ii). In these diagrams the intermediate lepton has one preon reversed, and the first two diagrams therefore yield factors of  $\alpha/(6\pi)$  rather than  $\alpha/(2\pi)$ . In conjunction with negation of the Standard Model corrections, they therefore yield a net correction to the QL scalar term with weight

$$-\frac{2\alpha q_\ell^2}{3\pi e^2}. \quad (61)$$

The third diagram is consistent with the Standard Model equivalent and so once again does not contribute to  $m_{\ell_i}$ .

Finally, there are two more diagrams from the scalar boson sector to consider. Moving a single scalar boson vertex onto the photon loop is prohibited as the diagram as a whole does not then leave the preon triplet unchanged (one preon gets replaced by an antipreon), but moving both vertices onto the loop is admissible. This results in the diagrams shown in Fig. 13(iii), of which only the second is anticipated to be non-vanishing by the arguments of Ref. 1, Sec. III F 3. This loop contributes to the mass of the loop photon (which vanishes by gauge), but also affects the fermion propagator to which it contributes a correction with weight  $\alpha/(2\pi)$  to the scalar boson term, combining with the above factor (61) to yield a correction of

$$\left(1 - \frac{\alpha q_\ell^2}{6\pi e^2}\right). \quad (62)$$

The net expression for lepton mass is thus

$$m_{\ell_i}^2 = f^2 \left[ k_i^{(\ell)} \right]^4 \left[ \mathcal{E}_{\text{QL}}^{(2)} \right]^2 \times \left\{ \frac{q_\ell^2}{e^2} + \frac{5m_{\ell_i}^2}{(m_c^*)^2} + \frac{240m_{\ell_i}^2 m_{\ell_1}^2}{\left[ k_1^{(\ell)} \right]^4 m_{\text{H}}^2 m_{\text{W}}^2} \left(1 - \frac{\alpha q_\ell^2}{6\pi e^2}\right) \right\} \quad (63)$$

but the final factor of

$$\left(1 - \frac{\alpha q_\ell^2}{6\pi e^2}\right) \quad (64)$$

is on the same scale as the  $O(\alpha)$  term in Eq. (56) and so may be dropped, as its most significant contribution is likewise only to  $m_Z$  at  $O(10^{-3} \sigma_{\text{exp}})$  (and in relative terms, to  $m_W$ ,  $m_Z$ , and  $m_{\text{H}}$  to order of parts in  $10^8$ ).

## 2. 1-loop gluon corrections

The next loop corrections to consider are those arising from gluon loops, analogous to the diagrams of Fig. 13. These gluons are foreground particles capable of making excursions outside of the local autocorrelation zone, and hence are massive, but the length scale involved is of order  $\mathcal{L}_\Psi$  so self-energy terms may be neglected, and the gluon loops exhibit at most only the bare gluon mass

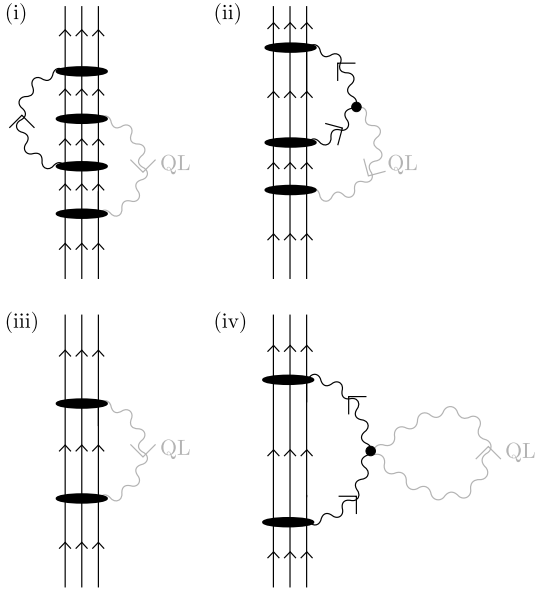


FIG. 15. (i)-(ii) Gluon loop equivalents to the first diagram of Fig. 13(i). When the fermion couples to the QL photon field, only diagram (i) may be constructed as the gluon does not carry an electromagnetic charge. When the fermion couples to the QL gluon field, both diagram (i) and diagram (ii) may be constructed. Conservation of colour charge indicates that on summing the coupling of the QL gluon to the fermion and the QL gluon to the loop gluon, this is equal to the coupling of the QL gluon to the fermion in the original leading-order diagram (iii). Similarly, diagram (iv) is the counterpart to the third diagram of Fig. 13(i). This diagram is especially interesting as it contributes both to the fermion mass and to the mass of the loop gluon. Note that the two QL gluons must couple with the loop gluon at a single vertex, as discussed in Ref. 1, Sec. III F 3.

(including the gluon deficit correction). Only loop corrections to the QL photon and QL gluon interactions need be considered in the present paper; corrections to the QL scalar boson interaction contribute to  $m_Z$  at  $O(10^{-3} \sigma_{\text{exp}})$  (in relative terms, to  $m_W$ ,  $m_Z$ , and  $m_H$  at parts in  $10^8$ ) and are therefore ignored.

Consider the gluon loop counterparts to Fig. 13(i). Where the fermion interacts with the QL photon field, these corrections take on the form of Fig. 15(i). For interactions between the fermion and the QL gluon fields they may take on the form of either Fig. 15(i) or (ii), and conservation of colour charge indicates that when these couplings are summed, this is equal to the coupling of the QL gluon to the fermion in the original leading-order diagram [Fig. 15(iii)]. Further, when the loop correction is evaluated, this collapses to a numerical multiplier on the original QL interaction vertex and the customary application of spinor identities [1, (170–171)] yields a non-vanishing contribution to  $m_{\ell_i}^2$ . It then suffices to consider an example where the coupling of the QL gluon and loop gluon vanishes, making it equivalent to the QL photon case, evaluate the correction to the interaction

vertex, and extrapolate this across all gluon colour combinations by  $GL(3, \mathbb{R})$  symmetry.

Figure 15(iv) shows a further diagram which may be constructed using gluon loop corrections. This is a counterpart to the gluon version of the third diagram of Fig. 13(i), and also contributes to the mass of the loop gluon.

Note that in contrast to the photon terms, where the third diagram of Fig. 13(i) was accounted for in the Standard Model, for preon/gluon interactions all loop corrections must be evaluated as there are no corresponding Standard Model terms.

To evaluate these corrections begin with Fig. 15(i), which is the gluon loop counterpart to Fig. 13(i). Start with the fermion coupling to the QL photon field, and a specific choice of off-diagonal gluon. Compare with the equivalent EM loop figure and note the following changes:

- The vertex factors increase from  $f^2/2$  to  $f^2$ , for a relative factor of two.
- The boson is off-diagonal, for a structural factor of  $\frac{5}{3}$ .
- The photon source may be any of three charged preons, but the gluon may only be emitted by a preon of appropriate colour. However, any of the three preons may be the preon of that colour, for a net factor of one.
- Emission of the off-diagonal gluon changes the colour of the emitting preon. There are then two preons of that colour which are capable of absorbing the loop gluon, and both of the resulting diagrams count as loop corrections due to the implicit exchange (not shown) of further gluons as a binding interaction sharing momentum between all members of the preon triplet. The choice of absorbing preons gives a factor of two.
- The loop gluon is massive, and is in the presence of a foreground fermion so experiences a gluon field mass deficit giving a loop factor of  $m_{\ell_i}^2/(m_c^*)^2$ .
- These factors multiply the equivalent photon loop factor, which is  $\alpha/(2\pi)$ .

The per-gluon correction weight from this diagram is therefore

$$\frac{10\alpha}{3\pi} \frac{m_{\ell_i}^2}{(m_c^*)^2}. \quad (65)$$

This calculation is repeated for the gluon counterparts to the other two figures of Fig. 13(i), and each of these figures may involve any of nine gluons, for a total weight of

$$\frac{90\alpha}{\pi} \frac{m_{\ell_i}^2}{(m_c^*)^2}. \quad (66)$$

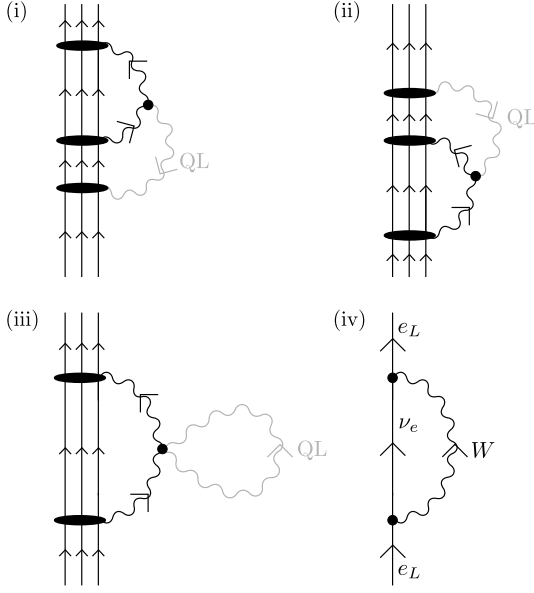


FIG. 16. (i)-(iii)  $W$  boson loop corrections to the QL vector boson interactions (QL photon or QL gluon). For QL photon terms, ignore the orientation arrows on the QL boson lines. (iv) Loop involving a  $W$  boson and a neutrino, appearing in the proper self-energy corrections of the Standard Model.

Correction of the QL gluon interactions proceeds equivalently, and as noted above the correction to the scalar boson may be ignored at current precision, for a net lepton mass so far of

$$m_{\ell_i}^2 = f^2 \left[ k_i^{(\ell)} \right]^4 \left[ \mathcal{E}_{\text{QL}}^{(2)} \right]^2 \quad (67)$$

$$\times \left\{ \frac{q_\ell^2}{e^2} \left[ 1 + \frac{90\alpha m_{\ell_i}^2}{\pi(m_c^*)^2} \right] + \frac{5m_{\ell_i}^2}{(m_c^*)^2} \left[ 1 + \frac{90\alpha m_{\ell_i}^2}{\pi(m_c^*)^2} \right] + \frac{240m_{\ell_i}^2 m_{\ell_1}^2}{\left[ k_1^{(\ell)} \right]^4 m_{\text{H}}^2 m_W^2} \right\}.$$

### 3. 1-loop weak force corrections

In the interest of brevity, this Section specialises to the charged leptons only.

*a. QL photon interaction:* When the fermion interacts with the QL photon field,  $W$  boson loops may correct this interaction as shown in Fig. 16. As with the gluon loops in Sec. IIIB2, the boson loops may be collapsed to numerical factors on the vertices of the corresponding leading-order diagram, and the QL field terms contracted using spinor/sigma matrix identities.

Some caution is required with sign—first consider diagram (iii). Evaluating this diagram as a tensor network in the manner of Ref. 4–6, it is readily seen to be an absolute square and therefore yields a contribution to  $m_{\ell_i}^2$  which is additive to the leading order term. Diagrams (i) and (ii) contain as a subdiagram a correction to the EM

emission process which is usually associated with the opposite sign to direct emission by the fermion; however, compared with diagram (iii) they have also acquired an additional fermion propagator segment which offsets this, so they are also additive. Relative to the leading-order diagram, Figs. 16(i)-(ii) acquire factors

- $(10/3)(m_{\ell_i}^2/m_W^2)$ , being the usual factor for a  $W$  loop correction to an EM vertex,
- $1/2$  due to loss of exchange symmetry for the two QL photon/composite fermion interactions. (Even with a composite fermion, an effective vertex is defined on summing over all possible preon/photon pairings and when identical, these effective vertices may still be exchanged for a symmetry factor of two.)

Diagram (iii) retains the exchange symmetry, this time on the two copies of the photon operator at the vertex, so attracts the factor of  $(10/3)(m_{\ell_i}^2/m_W^2)$  only.

Finally, consider the Standard Model counterpart: The charged lepton Proper Self-Energy (PSE) terms in the Standard Model give rise to the  $W$ /neutrino loop shown in Fig. 16(iv). This gives rise to a term analogous to Fig. 16(iii), but has no counterpart to the symmetry factor associated with the pair of identical photon operators on the QL interaction vertex. Its associated factor is therefore  $(5/3)(m_{\ell_i}^2/m_W^2)$ , which must be deducted. The net weight of the  $W$  boson loop corrections is thus

$$\frac{5\alpha m_{\ell_i}^2}{2\pi m_W^2}. \quad (68)$$

Next considering the  $Z$  boson loops, these take form directly analogous to Fig. 13, and by arguments similar to the above are also seen to all be additive. Noting that the  $Z$  boson couples with opposite sign to  $e_L$  and  $e_R$ , the  $Z$  boson equivalents to the first two diagrams of Fig. 13(i) are therefore of opposite sign to their Standard Model counterparts and hence attract a factor of two, to first offset the Standard Model-derived term in the PSE, and then implement the actual correction. The third diagram of Fig. 13(i), on the other hand, has the same sign as its Standard Model counterpart and thus yields no net contribution to  $m_{\ell_i}^2$ . The net outcome from  $Z$  boson loops is a term with weight

$$- \frac{4f_Z \alpha m_{\ell_i}^2}{2\pi m_W^2} \quad (69)$$

where  $f_Z$  is as defined in Eq. (19). Overall, the weight of the weak boson corrections to the QL photon interaction is seen to be

$$\frac{(5 - 4f_Z)\alpha m_{\ell_i}^2}{2\pi m_W^2}. \quad (70)$$

Note that the use of  $f_Z$ , which is dependent on the weak boson masses, implicitly incorporates the loop corrections to  $W$  and  $Z$  boson vertex interaction strengths.

This value is based on the mean  $Z$  vertex interaction strength, evaluated as a weighted average across all species which interact with the  $Z$  boson, but this approximation does not have a significant effect on the numerical results obtained, being responsible for corrections to  $m_Z$  at  $O(10^{-2} \sigma_{\text{exp}})$  (in relative terms, parts in  $10^8$  on  $m_W$ ,  $m_Z$ , and  $m_{H'}$ ).

*b. QL gluon interactions:* This term is readily obtained, as the calculation proceeds similarly to Sec. III B 3 a, and it is found to be right at the threshold of relevance. It is larger by a factor of 5 than the largest terms which have not been retained, and corrects  $m_Z$  at  $0.18 \sigma_{\text{exp}}$ .

As usual, start with the fermion interaction with a single off-diagonal QL gluon channel and then use  $GL(3, \mathbb{R})$  symmetry to multiply by nine for the contributions of the other eight gluons. For the gluon channels, the QL gluons continue to couple to the fermion and not the looping  $W$  boson, so when evaluating the equivalents of Figs. 16(i)-(ii) there is no factor of  $\frac{1}{2}$  for lost symmetry. The calculation is otherwise equivalent, for net  $W$  and  $Z$  corrections of

$$\frac{(25 - 12f_Z)\alpha m_{\ell_i}^2}{6\pi m_W^2}. \quad (71)$$

*c. QL scalar boson interaction:* These terms fall below the threshold of reliable evaluation with current numerical methods employed, with the largest correction appearing to be approximately  $10^{-11} \sigma_{\text{exp}}$  on  $m_\tau$ , or parts in  $10^{16}$ .

The cumulative expression for charged lepton mass incorporating weak boson corrections is therefore

$$\begin{aligned} m_{\ell_i}^2 = & f^2 \left[ k_i^{(\ell)} \right]^4 \left[ \mathcal{E}_{\text{QL}}^{(2)} \right]^2 \\ & \times \left\{ \left[ 1 + \frac{90\alpha m_{\ell_i}^2}{\pi(m_c^*)^2} + \frac{(5 - 4f_Z)\alpha m_{\ell_i}^2}{2\pi m_W^2} \right] \right. \\ & + \frac{5m_{\ell_i}^2}{(m_c^*)^2} \left[ 1 + \frac{90\alpha m_{\ell_i}^2}{\pi(m_c^*)^2} + \frac{(25 - 12f_Z)\alpha m_{\ell_i}^2}{6\pi m_W^2} \right] \\ & \left. + \frac{240m_{\ell_i}^2 m_{\ell_1}^2}{\left[ k_1^{(\ell)} \right]^4 m_{H'}^2 m_W^2} \right\}. \end{aligned} \quad (72)$$

#### 4. 1-loop scalar corrections

These terms fall below the threshold of relevance, leading to corrections to  $m_Z$  at  $O(10^{-2} \sigma_{\text{exp}})$ , or in relative terms, to  $m_W$ ,  $m_Z$ , and  $m_{H'}$  at approximate order of parts in  $10^7$ .

#### 5. 2-loop EM corrections

These terms fall below the threshold of relevance, leading to corrections to  $m_Z$  at  $O(10^{-3} \sigma_{\text{exp}})$ , or in relative

terms, to  $m_\tau$  at approximate order of parts in  $10^8$ .

## C. Corrections to the lepton mass angle

### 1. Origin of corrections

There remains one more substantial correction to evaluate. The leading-order contributions to the lepton mass vertices and the preon colour mixing matrix were evaluated in Sec. III A. Loop corrections to the mass vertices were evaluated in Sec. III B. It remains now to determine how these loop corrections impact the preon colour mixing matrix  $K_\ell$ .

When this matrix was constructed in Sec. III A 1 there was an implicit assumption that all eigenvectors experience equal couplings to the QL fields. The eigenvalues of matrix  $K_\ell$  then imparted different masses to the three eigenvectors, corresponding to the three members of a given fermion family. However, from Eq. (72) it is apparent that the higher-order corrections to the QL coupling themselves depend on particle mass, leading to differential augmentation of the three eigenvectors (mass channels). As these eigenvectors correspond to different vectors in colour space, imparting different relative phases to the gluon couplings between the preon triplets, a change in the relative QL couplings for the different eigenvectors will impact the colour mixing process. Conveniently, it proves possible to represent this modification by a correction to the value of  $\theta_\ell$ .

Recognising that the fermion masses vary between different particle families, it is necessary to specify the family for which the corrected value of  $\theta_\ell$  is being evaluated. This is done by replacing  $\ell$  with a member of the particle family in question, e.g.  $e$ ,  $\mu$ , or  $\tau$  for the electron family.

### 2. Preamble

To obtain a corrected expression for the electron mass angle at some energy scale  $\mathcal{E}$ , first recall that the eigenvectors  $\{v_i | i \in \{1, 2, 3\}\}$  of  $K_\ell$  (49–51) are independent of the value of  $\theta_\ell$ . For the electron family, matrix  $K_\ell$  therefore always admits the decomposition

$$K_\ell = \sum_{i=1}^3 k_i^{(\ell)} v_i v_i^\dagger \quad (73)$$

where

$$v_1 v_1^\dagger = \frac{1}{3} \begin{pmatrix} 1 & 1 & 1 \\ 1 & 1 & 1 \\ 1 & 1 & 1 \end{pmatrix} \quad (74)$$

$$v_2 v_2^\dagger = \frac{1}{3} \begin{pmatrix} 1 & e^{-\frac{2\pi i}{3}} & e^{-\frac{2\pi i}{3}} \\ e^{-\frac{2\pi i}{3}} & 1 & e^{-\frac{2\pi i}{3}} \\ e^{-\frac{2\pi i}{3}} & e^{-\frac{2\pi i}{3}} & 1 \end{pmatrix} \quad (75)$$

$$v_3 v_3^\dagger = \frac{1}{3} \begin{pmatrix} 1 & e^{-\frac{2\pi i}{3}} & e^{-\frac{2\pi i}{3}} \\ e^{-\frac{2\pi i}{3}} & 1 & e^{-\frac{2\pi i}{3}} \\ e^{-\frac{2\pi i}{3}} & e^{-\frac{2\pi i}{3}} & 1 \end{pmatrix}. \quad (76)$$

Then note that the imaginary components of the off-diagonal matrix elements arise from components 2 and 3 only (75–76), with an increase in component 2 (corresponding, for charged leptons, to the muon) making a positive-signed contribution to the imaginary component in  $[K_\ell]_{12}$ ,  $[K_\ell]_{23}$ , and  $[K_\ell]_{31}$ . Examining the vectors on the complex plane associated with  $\exp(\theta_e) = \exp(-3\pi i/4)$  and a small correction proportional to  $\exp(2\pi i/3)$ , it is seen that the action of this correction is to increase the magnitude of  $\theta_\ell$  (making it more negative). Similarly, an isolated increase in component 3 (the tau) decreases  $\theta_\ell$ . Finally, an isolated increase in component 1 (the electron) affects only the real component of an entry such as  $[K_\ell]_{12}$  and thus when  $[K_\ell]_{12}$  is complex, once again affects the value of  $\theta_\ell$ . When  $\theta_\ell$  is no longer fixed to be  $-3\pi/4$ , it is labelled by the relevant particle family, e.g.  $\theta_e$ , and it becomes necessary to specify  $K_\ell$  as  $K_\ell(\theta_\ell)$  for some family  $\ell$ .

Next, recognise that it is convenient to write the mass interaction as a leading-order term derived from the QL photon field (and associated with colour mixing matrix  $K_\ell$  as derived Sec. III A 1) plus corrections. For the charged lepton masses, this corresponds to rewriting Eq. (72) as

$$m_{e_i}^2 = f^2 \left[ k_i^{(e)} \right]^4 \left[ \mathcal{E}_{\text{QL}}^{(2)} \right]^2 \left[ 1 + \Delta_e(m_{e_i}) \right] \\ = \left[ m_{e_i}^{(0)} \right]^2 \left[ 1 + \Delta_e(m_{e_i}) \right] \quad (77)$$

$$\Delta_e(m_{e_i}) = \frac{90\alpha m_{e_i}^2}{\pi(m_c^*)^2} + \frac{(5 - 4f_Z)\alpha m_{e_i}^2}{2\pi m_W^2} \\ + \frac{5m_{e_i}^2}{(m_c^*)^2} \left[ 1 + \frac{90\alpha m_{e_i}^2}{\pi(m_c^*)^2} + \frac{(25 - 12f_Z)\alpha m_{e_i}^2}{6\pi m_W^2} \right] \\ + \frac{240m_{e_i}^2 m_{e_1}^2}{\left[ k_1^{(e)} \right]^4 m_{\text{H}}^2 m_W^2} \quad (78)$$

where  $\{e_1, e_2, e_3\} = \{e, \mu, \tau\}$  and the subscript  $e$  on  $\Delta_e$  indicates the family  $\{e, \mu, \tau\}$  rather than the electron in particular. As can be readily seen from Eq. (78), the amplitudes of these corrections to particle mass are dependent upon the squared lepton masses  $m_{e_i}^2$ , with the

largest corrections being those associated with the tau. The charged lepton mixing matrix  $K_e(\theta_e)$  is implicitly dependent on the same corrections, as changes to the particle mass ratios affect colour mixing, and hence the co-ordinate transformation required to restore colour neutrality. Allowing the corrections to augment mass and also to adjust  $K_e(\theta_e)$  is not double-counting, as the mass correction *induces* the corresponding adjustment in the co-ordinate transformation implemented by  $K_e(\theta_e)$ . The co-ordinate transformation does, however, have an effect on the magnitude of the mass correction term, and this effect must be compensated for—see Sec. III C 5.

### 3. First-order correction to $K_\ell^4$ from the tau channel

To understand how these corrections to lepton masses affect the matrices  $K_\ell$ , consider the leading order term  $[m_{e_i}^{(0)}]^2$  which arises from the set of nine diagrams described in the caption of Fig. 10, and may be thought of as the action of an operator  $[\hat{m}^{(0)}]^2$  on the preon triplet comprising a sum over nine terms. The action of this operator on the colour space of the preon triplet breaks colour neutrality, but this is then corrected by application term-by-term of four matrices (or operators)  $K_\ell$ , heuristically  $K_\ell^4$  (with implicit action of each operator on the appropriate Hilbert space as per the appropriate diagram of Fig. 10), such that  $K_\ell^4 [\hat{m}^{(0)}]^2$  as a whole leaves the colour of the preon triplet unchanged up to a cycle  $r \rightarrow g \rightarrow b \rightarrow r$ .

As seen in Eq. (77), higher-order corrections enhance the action of  $[\hat{m}^{(0)}]^2$  on eigenstate  $e_i$  by a factor of  $[1 + \Delta_e(m_{e_i})]$ . If colour neutrality is to be conserved, then for colour-changing diagrams [including those which *can* mix colours under some global  $\text{SU}(3)_C$  transformation, such as interaction with the diagonal gluons of the **8** representation of  $\text{SU}(3)_C$ ] there must be an equivalent enhancement of the matrices  $K_\ell$ ,

$$K_\ell \rightarrow K_e(\theta_e) \quad (79)$$

[where dependence on  $\theta_e(\{m_{e_i}|i \in \{1, 2, 3\}\})$  is assumed but will subsequently be shown] such that the action of  $[K_e(\theta_e)]^4$  on  $e_i$  is equivalent to the action of  $K_\ell^4 [1 + \Delta_e(m_{e_i})]$ .

As the largest such correction arises from the most massive particle, begin by considering  $e_3$ , the tau. First note that introduction of a mass dependency for the matrices  $K_e(\theta_e)$  implies that the bosons associated with the colour-neutrality-preserving co-ordinate transformation are no longer parameterless, and may therefore carry momentum in the higher-order diagrams. They must therefore be represented explicitly as per Fig. 17. By construction these bosons only interact at the boundary of the transformed co-ordinate patch, and are consequently both foreground and massless. Let the diagrams of Fig. 17(i)-(iii), having two co-ordinate transformation bosons, be termed “first order”, and for now

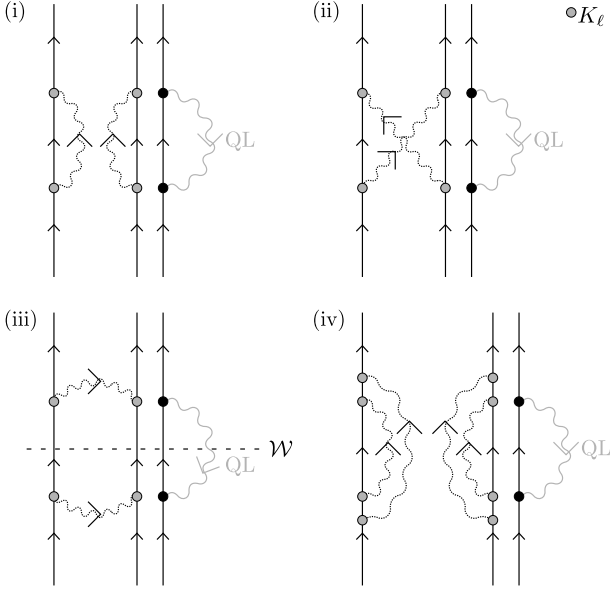


FIG. 17. When the matrices  $K_\ell$  are replaced by  $K_e(\theta_e)$ , which depends on energy scale, this induces a pair of gauge bosons which may in principle connect the four matrices  $K_e(\theta_e)$  in any of three ways [shown for Fig. 10(i) in diagrams (i)-(iii)]. In diagram (i), the bosons each connect to two matrices  $K_e(\theta_e)$  on the same preon and thus enact a co-ordinate transformation followed by its inverse. In diagram (ii), where the bosons are crossed, there may be a permutation of the preon colour labels but overall colour neutrality is nevertheless conserved. Diagram (iii) contrasts with the other two in that the boson trajectories are orthogonal to the preon trajectories. For a worldsheet such as that shown (labelled  $\mathcal{W}$ ), which is equidistant between the boson vertices and isochronous in the rest frame of the particle, the total number of oriented crossings for each of the bosons in diagram (iii) is zero regardless of the trajectory followed. This implies that these bosons do not describe a co-ordinate transformation extant at this worldsheet, and thus this diagram does not contribute to  $K_e(\theta_e)$ . Diagram (iv) is an example second-order diagram having four bosons arising from the co-ordinate transformation and spanning from the lower to the upper collection of matrices  $K_e(\theta_e)$ . This diagram represents the consecutive application of two (possibly different) transformations in  $SU(3)_C$  to each preon.

ignore diagrams having four co-ordinate transformation bosons (“second order”).

Regarding the two co-ordinate transformation bosons of Fig. 17(i)-(ii), their vertex factors are incorporated into the leading order matrix  $K_\ell$ . Integration over their degrees of freedom then yields a factor per diagram of  $(4\pi)^{-2}$  [not  $(2\pi)^{-2}$ , as they are not self-dual and thus their loop is less symmetric than that for the photon]. Note that Fig. 17(ii) counts as a loop diagram as there are implicit gluon-mediated couplings between the preonic constituents of the lepton, which are massless over the length-scale involved [ $O(\mathcal{L}_{QL})$ ] and complete closure of the loop.

Recognising that the leading term calculation does not

perform any net colour mixing beyond the unmodified, constant factors of  $K_\ell^4$ , the resulting factor of  $2 \cdot (4\pi)^{-2}$  does not appear in the leading term calculation. Its effect is seen only on the diagrams in  $\Delta_e(m_\tau)$ , where it represents variations in colour mixing relative to  $K_\ell^4$ , and multiplies any correction to  $K_\ell^4$  by a factor of  $2 \cdot (4\pi)^{-2}$ .

Next, recognise that the components of each matrix  $K_e(\theta_e)$  which perform rotations on  $SU(3)_C$  are composed from a weighted superposition of some set of representation matrices  $\lambda'_i$  (possibly, but not necessarily the matrices  $\lambda_i$  of Appendix A), of which there are eight. (A ninth basis element is associated with the trivial representation and acts to preserve norm, but is strictly diagonal, and independent of  $\theta_e$ , so is not yet of interest here.) An appropriate choice of basis permits every off-diagonal element in  $K_e(\theta_e)$  to be associated with a single basis element {for example, in  $K_\ell$ , entry  $[K_\ell]_{12}$  is associated with  $(\lambda_1 + \lambda_2)/\sqrt{2}$ }. A change to  $\theta_e$  may correspond to a change in choice of representation matrices [e.g. to  $\lambda_1 \cos \beta + \lambda_2 \sin \beta$  for some angle  $\beta$ ] but this ability to construct a single basis element corresponding to a particular entry in  $K_e(\theta_e)$  persists for any reasonably small perturbation around  $\theta_e = -3\pi/4$ .

Now consider a preon in Fig. 10(i) or (ii) which has two matrices  $K_e(\theta_e)$  acting on it, and recognise that if the portion of  $K_e(\theta_e)$  which performs colour transformations is decomposed into these eight components, then if a given component  $\lambda'_i$  acts on the preon in the lower position, then its conjugate must act in the upper position for the foreground preon colour to be left invariant overall.<sup>3</sup> The action of the *pair* of matrices  $K_e(\theta_e)$  on this boson consequently admits decomposition into eight channels, enumerated by the family of orthogonal representation matrices  $\lambda'_i$  appearing at the lower matrix  $K_e(\theta_e)$ .

Next, consider the remaining two matrices  $K_e(\theta_e)$  when these are not on the same preon. In this situation the representation matrices present will be conjugate up to a colour cycle  $r \rightarrow g \rightarrow b \rightarrow r$  or its inverse. As the only colour-changing bosons in the QL are gluons, and  $SU(3)_C$  symmetry is preserved on the gluon sector and in the definition of the charged lepton, evaluation of any diagram where the entries from  $K_e(\theta_e)$  are offset by a colour cycle is necessarily equivalent to evaluation of a diagram where they are not offset. It is therefore acceptable

<sup>3</sup> Note that if one diagram family as per Fig. 10 can be made to have no net effect on colour, then all paired QL bosons have no net effect on colour. Further, as unpaired bosons (as well as being exceedingly rare) have on average no net effect on colour, these may also be grouped into clusters having zero net colour effect overall, and an analogous co-ordinate transformation performed such that their effect on colour vanishes instant-by-instant as well as on average, with the associated bosons vanishing over distances large compared with  $\mathcal{L}_{QL}$ . Thus no error is made in requiring that colour is left unchanged on a per-diagram basis. Also note that once the mechanism for corrections to  $\theta_e$  is fully elucidated, the co-ordinate transformations arising from the unpaired bosons yield no systematic effect on  $\theta_e$  and thus their effect may be ignored over macroscopic scales.

to evaluate entries in  $K_e(\theta_e)$  under the assumption that all matrices  $K_e(\theta_e)$  appear in conjugate pairs. In addition, in all diagrams all representation matrices are multiplied by their conjugate (whether independently or in conjunction with the representation matrices associated with the bosonic vertices) and thus the terms arising from all 64 channels contributing to the actions of the matrices  $K_e(\theta_e)$  on the preon triplet are additive on the same (net trivial) charge sector, and therefore summed. By  $SU(3)_C$  symmetry, each channel will contribute equally to the overall correction to the leading order diagram.

Now consider the single channel associated with a specific off-diagonal entry in at least one lower matrix  $K_e(\theta_e)$ . For definiteness, let this be  $[K_e(\theta_e)]_{12}$ . As there are, overall, 64 contributing channels, each channel must produce a net correction of  $\Delta_e(m_\tau)/64$ . However, the synthetic bosons multiply all correction diagrams by a factor of  $2 \cdot (4\pi)^{-2}$  and thus  $[K_e(\theta_e)]_{12}$  and  $[K_e(\theta_e)]_{21}$  must satisfy

$$\begin{aligned} [K_e(\theta_e)]_{12}^2 [K_e(\theta_e)]_{21}^2 &= [K_\ell]_{12}^2 [K_\ell]_{21}^2 \left[ 1 + \frac{(4\pi)^2}{2 \cdot 64} \Delta_e(m_\tau) \right] \\ &= [K_\ell]_{12}^2 [K_\ell]_{21}^2 \left[ 1 + \frac{\pi^2}{8} \Delta_e(m_\tau) \right] \end{aligned} \quad (80)$$

$$\Rightarrow [K_e(\theta_e)]_{12} [K_e(\theta_e)]_{21} = [K_\ell]_{12} [K_\ell]_{21} \sqrt{1 + \frac{\pi^2}{8} \Delta_e(m_\tau)}. \quad (81)$$

Noting that  $[K_\ell]_{12} = [K_\ell]_{21}^\dagger$ , it is convenient to write

$$\delta_e(n) = \sqrt{1 + \frac{\pi^2 n}{8}} - 1 \quad (82)$$

$$[1 + \delta_e(n)] = [1 + i\sqrt{\delta_e(n)}][1 - i\sqrt{\delta_e(n)}] \quad (83)$$

and assign the corresponding off-diagonal entries of  $K_e(\theta_e)$  to be

$$\begin{aligned} [K_e(\theta_e)]_{12} &= [K_\ell]_{12} [1 \pm i\sqrt{\delta_e[\Delta_e(m_\tau)]}] \\ [K_e(\theta_e)]_{21} &= [K_\ell]_{21} [1 \mp i\sqrt{\delta_e[\Delta_e(m_\tau)]}], \end{aligned} \quad (84)$$

preserving the Hermiticity of  $K_e(\theta_e)$ .

By the factor of  $\pm i$  on the correction term, this correction is orthogonal to the leading-order value of  $[K_\ell]_{12}$ . As this orthogonality is independent of the value of  $\theta_e$ , this implies that for a non-infinitesimal correction,  $\sqrt{\delta_e[\Delta_e(m_\tau)]}$  is the length of an arc. Since  $[K_\ell]_{12}$  is of unit length, the corresponding correction to  $\theta_\ell$  is

$$\theta_\ell \rightarrow \theta_\ell \pm \sqrt{\delta_e[\Delta_e(m_\tau)]} + O(\{\delta_e[\Delta_e(m_\tau)]\}^{\frac{3}{2}}). \quad (85)$$

In the vicinity of  $\theta_\ell = -3\pi/4$ , this may be rewritten

$$\theta_\ell \rightarrow \theta_\ell \left\{ 1 \mp \frac{4\sqrt{\delta_e[\Delta_e(m_\tau)]}}{3\pi} \right\}. \quad (86)$$

As per the discussion under Eqs. (74–76), the tau correction is known to decrease the magnitude of  $\theta_\ell$ , giving

$$[K_e(\theta_e)]_{12} = \frac{e^{i\theta_e}}{\sqrt{2}} = [K_\ell]_{12} \left\{ 1 + i\sqrt{\delta_e[\Delta_e(m_\tau)]} \right\} \quad (87)$$

$$\theta_e = -\frac{3\pi}{4} \left\{ 1 - \frac{4\sqrt{\delta_e[\Delta_e(m_\tau)]}}{3\pi} \right\} \quad (88)$$

where the value of  $\theta_\ell$  has been written explicitly as  $-\frac{3\pi}{4}$ .

#### 4. Second-order correction to $K_\ell^4$ from the tau channel

The first-order correction to  $K_\ell^4$  is applied to all diagrams which modify the colour mixing process, i.e. all diagrams contributing to  $\Delta_e$ . For these diagrams, this correction is equivalent by construction to enacting the transformation

$$K_\ell^4 \rightarrow K_\ell^4 [1 + \Delta_e(m_\tau)], \quad (89)$$

resulting in a relative increase in these diagrams' contribution to particle mass equivalent to

$$\Delta_e(m_\tau) \rightarrow \Delta_e(m_\tau)[1 + \Delta_e(m_\tau)]. \quad (90)$$

Any species-dependent increase in mass affects colour mixing in precisely the way described above for correction  $\Delta_e(m_\tau)$ , regardless of whether this increase is diagrammatic (as in the first-order component) or gauge-dependent and derived from a change to  $\theta_e$  (as here). This correction therefore attracts a further smaller correction to  $K_\ell$ , enhancing the first-order correction calculated above. While this series may be continued indefinitely, it is convenient to truncate at second order for a precision of  $O[\Delta_e^2(m_\tau)]$ .

To implement the corresponding adjustment to  $K_e(\theta_e)$ , let the  $O[\Delta_e^2(m_\tau)]$  term be compensated by the second-order diagrams of which Fig. 17(iv) is a prototype. In these diagrams, a first-order correction [Fig. 17(i)-(ii)] is supplemented by a further, smaller correction.

For Figs. 17(i)-(ii) there is a symmetry factor of two corresponding to crossing or not crossing the bosons. For Fig. 17(iv),

- the inner pair may be crossed (factor of two),
- the outer pair may be crossed (factor of two),
- the inner and outer bosons on the left may be exchanged (factor of two), and
- the inner and outer bosons on the right may be exchanged (factor of two).

The factor of  $2 \cdot (4\pi)^{-2}$  associated with the set of diagrams Figs. 17(i)-(ii) becomes a factor of  $16 \cdot (4\pi)^{-4}$  for the set

of diagrams derived from Fig. 17(iv). The expression for  $[K_e(\theta_e)]_{12}^2 [K_e(\theta_e)]_{21}^2$  then becomes

$$\begin{aligned} & [K_e(\theta_e)]_{12}^2 [K_e(\theta_e)]_{21}^2 \\ &= [K_\ell]_{12}^2 [K_\ell]_{21}^2 \left[ 1 + \frac{(4\pi)^2}{2 \cdot 64} \Delta_e(m_\tau) + \frac{(4\pi)^4}{16 \cdot 64^2} \right] \Delta_e^2(m_\tau) \\ &= [K_\ell]_{12}^2 [K_\ell]_{21}^2 \left\{ 1 + \frac{\pi^2}{8} \Delta_e(m_\tau) \left[ 1 + \frac{\pi^2}{32} \Delta_e(m_\tau) \right] \right\} \end{aligned} \quad (91)$$

for a redefinition of  $\delta_e(n)$  in Eq. (88) to

$$\delta_e(n) = \sqrt{1 + \frac{\pi^2 n}{8} \left( 1 + \frac{\pi^2 n}{32} \right)} - 1. \quad (92)$$

The next order term extends  $\delta_e(n)$  to

$$\delta_e(n) = \sqrt{1 + \frac{\pi^2 n}{8} \left[ 1 + \frac{\pi^2 n}{32} \left( 1 + \frac{\pi^2 n}{72} \right) \right]} - 1 \quad (93)$$

but is not used in this paper as its effects fall below the threshold of relevance. Its most significant correction is to  $m_Z$  at  $O(10^{-2} \sigma_{\text{exp}})$ , or in relative terms, to  $m_W$ ,  $m_Z$ , and  $m_H$  in order of parts in  $10^7$ .

### 5. Dilaton corrections to $\Delta_e(m_{e_i})$

*a. Running of  $m_{e_i}$*  In Sec. III E 1 a of Ref. 1, the dilaton parameter was gauged by requiring normalisation of probabilities for all foreground particles. However, probability is a property normalised on integrating over a three-dimensional worldsheet in  $\mathbb{R}^{1,3}$ , whereas the dilaton coefficient may vary in time as well as space. With probability amplitudes depending only on  $x^i | i \in \{1, 2, 3\}$  but with the dilaton coefficient being a function of  $x^\mu$ , the dilaton gauge is therefore underconstrained. This choice of gauge may therefore be extended to normalise one further parameter, provided that parameter is energy/timelike and its rescaling is independent of the probability parameters being normalised over  $\mathbb{R}^3$ .

Now recognise that in the above, the lepton mass  $m_{e_i}$  has been written as a function of  $\Delta_e$  and  $\theta_e$ , which are in turn a function of both the lepton mass itself and also the energy scale of the gluon deficit. For a particle which is both on-shell and at rest, these two energy scales are identical, but more generally, the gluon mass deficit will run with energy scale. This running leads to a running of electron mass which has no counterpart in the Standard Model. Therefore complete the gauging of the dilaton parameter by enforcing that everywhere, after rescaling,  $\langle m_e^2 \rangle_{O(\mathcal{L}_{\text{QL}})}$  takes on its rest value regardless of the energy of the electron. The implications of this gauge will be seen in Sec. IV A.

*b. Rescaling arising from colour mixing* The above transformations have maintained colour neutrality, but

at the expense of introducing an additional scaling factor of  $[1 + \Delta_e(m_\tau)]$  on all diagrams which affect the colour mixing process [i.e. all diagrams in  $\Delta_e(m_\tau)$ ]. This rescaling is unphysical, being the result of a forced (non-gauge) change in local co-ordinate system, and may not in general be assumed to conserve the normalisation of probability and electron mass generated by the choice of dilaton gauge [1, Sec. III E 1 a; Sec. III C 5 a above]. This then induces a change in the dilaton gauge which rescales the affected sector to eliminate this factor.

The effect of this change of gauge on particle mass is to rescale the modified correction factor

$$\begin{aligned} \Delta_e(m_\tau)[1 + \Delta_e(m_\tau)] &\rightarrow \Delta_e(m_\tau)[1 + \Delta_e(m_\tau)][1 + \Delta_e(m_\tau)]^{-1} \\ &= \Delta_e(m_\tau) \end{aligned} \quad (94)$$

recovering a particle mass of

$$m_\tau^2 = [m_e^{(0)}]^2 [1 + \Delta_e(m_\tau)]. \quad (95)$$

This correction factor of  $[1 + \Delta_e(m_\tau)]^{-1}$  arises from the dilaton field and thus is insensitive to colour charge. In contrast, the calculation of  $\theta_e$  is performed on a single channel of  $SU(3)_C$ , and thus on a single channel of  $GL(3, \mathbb{R})$ . Recognising that the correction  $\Delta_e(m_\tau)$  to particle mass arises from a symmetric sum over all nine channels of  $GL(3, \mathbb{R})$ , it consequently follows that the calculation of  $\theta_e$  ‘‘sees’’ only one ninth of the total correction arising from the regauging of the dilaton field.

Further recognise that to maintain colour neutrality this correction factor must be partitioned equally between the mass interaction and the compensatory matrices  $[K_e(\theta_e)]^4$ . The result is to rescale  $\Delta_e(m_\tau)$  in Eq. (88) according to  $\Delta_e(m_\tau) \rightarrow r[\Delta_e(m_\tau)]$ ,

$$\begin{aligned} \theta_e = -\frac{3\pi}{4} \left\{ 1 - \frac{4\sqrt{\delta_e\{r[\Delta_e(m_\tau)]\}}}{3\pi} \right. \\ \left. + O\left[\left(\delta_e\{r[\Delta_e(m_\tau)]\}\right)^{\frac{3}{2}}\right] \right\} \end{aligned} \quad (88b)$$

$$r(n) = n \cdot \sqrt{1 + \frac{(1+n)^{-1} - 1}{9}}, \quad (96)$$

again to  $O[\Delta_e^2(m_\tau)]$ .

### 6. Corrections to $[K_e(\theta_e)]^4$ from the muon and electron channels

Now recognise that a propagating preon is a massive particle and undergoes multiple scatterings off the QL fields. These scatterings may impart energy to or take energy from the preon, and are generally ignored as their average contributions vanish over length scales large compared with  $\mathcal{L}_{\text{QL}}$ . Bringing these into consideration, it is necessary to integrate over all possible scatterings of

the preon off the QL fields, and for a foreground preon with a rest energy small compared with  $\mathcal{E}_{\text{QL}}$ , the net effect is to integrate near-homogeneously over all energies from  $-\mathcal{E}_{\text{QL}}$  to  $+\mathcal{E}_{\text{QL}}$  [effectively homogeneously at energies small compared with  $\mathcal{E}_{\text{QL}}$ , corresponding to boosts small compared with  $1 - 10^{32}$  as per Eq. (13)]. On-shell contributions appear at the three eigenvalues of  $K_e(\theta_e)$ , and thus even for a foreground lepton in a definite colour sector eigenstate, all three channels contribute to the correction to  $\theta_e$ . Over length scales of  $O(\mathcal{L}_{\text{QL}})$ , in expressions involving the matrices  $K_e(\theta_e)$ , particle propagation is summed over the three generation channels. In expressions which do not involve these matrices, such as evaluation of boson masses, fermion symbols are generationless. Evaluation of the parameter  $\theta_e$  inevitably involves the mixing matrices  $K_e(\theta_e)$ , and thus corrections to  $\theta_e$  from all channels of propagation must be considered regardless of the generation of the foreground particle which may be measured in the low-energy limit.

Now that there are multiple energy scales involved, it is advisable to be more careful with the gluon mass deficit. This also permits generalisation to particles further from rest in the isotropy frame of the QL, and is useful preparation for Sec. IV A, in which off-shell excitations are considered. Note that the mean energy scale of the gluon deficit is determined by the mean additional energy acquired by the foreground species on account of its nonzero rest mass, i.e.

$$[k_0]_{\text{fg}} - \sqrt{[k_1]_{\text{fg}}^2 + [k_2]_{\text{fg}}^2 + [k_3]_{\text{fg}}^2}, \quad (97)$$

and that this is not in general the same as the instantaneous energy of the propagating particle. The gluon deficit undergoes its own energy fluctuations around this value as a result of energy exchange between the deficit and the QL, but these are not necessarily simultaneous with the fluctuations of the representative foreground particle, and in the absence of any generations mechanism for bosons, may be separately averaged to zero. Further, when a particle is off-shell, or undergoes a boost relative to the QL, this affects the energy scale of the gluon deficit via Eq. (97) without affecting particle rest mass save through the dependency of rest mass on the gluon deficit as per Eq. (78). Recognising the independence of these energy scales, therefore write

$$\begin{aligned} \Delta_e(m_{e_i}, \mathcal{E}) &= \frac{90\alpha m_{e_i}^2}{\pi [m_c^*(\mathcal{E})]^2} + \frac{(5 - 4f_Z)\alpha m_{e_i}^2}{2\pi m_W^2} \\ &+ \frac{5m_{e_i}^2}{[m_c^*(\mathcal{E})]^2} \left[ 1 + \frac{90\alpha m_{e_i}^2}{\pi [m_c^*(\mathcal{E})]^2} + \frac{(25 - 12f_Z)\alpha m_{e_i}^2}{6\pi m_W^2} \right] \\ &+ \frac{240m_{e_i}^2 m_{e_1}^2}{[k_1^{(e)}]^4 m_H^2 m_W^2} \end{aligned} \quad (98)$$

$$[m_c^*(\mathcal{E})]^2 = m_c^2 \left( 1 - \frac{27}{10} \frac{\mathcal{E}^2}{m_c^2 c^4} \right), \quad (59b)$$

where  $\mathcal{E}$  is the energy scale used in calculation of the gluon mass deficit correction. Previous occurrences of

$\Delta_e(m_\tau)$  in Secs. III C 3–III C 5 are thus noted to implicitly be  $\Delta_e(m_\tau, m_\tau c^2)$ .

To evaluate the correction arising from the  $e_2$  or muon channel, recognise from Eqs. (75–76) that the effect of this correction is in opposition to the tau correction, and increases the magnitude of  $\theta_e$ . As its scale is seen from Eq. (78) to be small compared with the tau correction, and from the construction of Eq. (84) it is seen to act in direct opposition to the tau correction, its effects are conveniently represented at energy scale  $\mathcal{E}$  by subtracting the muon correction from the tau correction at the level of the interaction diagrams. This yields

$$\theta_e(\mathcal{E}) = -\frac{3\pi}{4} \left( 1 - \frac{4\sqrt{\delta_e} \{r[\Delta_e(m_\tau, \mathcal{E}) - \Delta_e(m_\mu, \mathcal{E})]\}}{3\pi} \right) \quad (99)$$

where  $\theta_e(\mathcal{E})$  is the effective value of  $\theta_e$  experienced by a particle whose mass is  $\mathcal{E}c^{-2}$ , and henceforth all instances of  $\theta_e$  are acknowledged to depend, either explicitly or implicitly, on a particle's energy scale  $\mathcal{E}$ .

Finally, the  $e_1$  or electron channel is seen from Eq. (74) to contribute purely to the real part of  $[K_e(\theta_e)]_{12}$ . For the imaginary part, all positive contributions to the imaginary portion of  $[K_e(\theta_e)]_{12}$  arise from the muon channel and all negative contributions from the tau channel, enabling the relatively simple form of Eq. (99). In contrast, while the electron channel contributes to the real part of  $[K_e(\theta_e)]_{12}$  the bulk of the real part (and, indeed, for  $\theta_\ell = -3\pi/4$  the entirety of the real part) arises instead from the muon and tau channels.

Let the electron mass undergo a rescaling  $m_e^2 \rightarrow m_e^2[1 + \Delta_e(m_e, \mathcal{E})]$ , resulting in some rescaling  $(1 + \varepsilon)$  of  $k_1^{(e)}$ . As the real and imaginary components of  $\exp(i\theta_\ell)$  are both negative, the increase in the real component of  $[v_1 v_1^\dagger]_{12}$  associated with this correction will decrease the magnitude of  $\theta_\ell$ . However, the electron mass is one of the fixed input parameters to the model, and consequently this rescaling (and its associated effect on  $\theta_\ell$ ) must be offset by a decrease in magnitude of the associated energy scale  $\mathcal{E}_{\text{QL}}^{(2)}$  {and thus of  $[m_e^{(0)}]^2$ } corresponding to multiplication by  $(1 + \varepsilon)^{-1}$ . If this value is pulled out as an independent factor, in the electron mass diagram it cancels with the  $(1 + \varepsilon)$  arising from the electron mass rescaling, leaving  $m_e$  and  $k_1$  unchanged (and eliminating any need to evaluate colour effects from this sector). However, for the muon and the tau it may be seen as a rescaling of  $k_2^{(e)}$  or  $k_3^{(e)}$  respectively by a factor of  $(1 + \varepsilon)^{-1}$ . To elucidate the effect of this scaling factor on  $\theta_\ell$ , restore colour neutrality by likewise holding the muon and tau masses fixed, corresponding to enacting a transformation

$$k_i^{(e)} \rightarrow k_i^{(e)}(1 + \varepsilon) \quad | \quad i \in \{2, 3\}. \quad (100)$$

The leading colour effect arising from this transformation is equivalent to a rescaling of  $k_3^{(e)}$  (which generates the leading correction to  $\theta_\ell$ ) by  $(1 + \varepsilon)$  and is therefore

associated with an *increase* in the magnitude of  $\theta_\ell$ . The rescaling of the muon term is by the same factor. This multiplier is independent of the existing muon and tau corrections, having its origins on the real rather than the imaginary portion of  $[K_e(\theta_e)]_{12}$ , and therefore must be evaluated as a separate correction to  $\theta_\ell = -3\pi/4$  rather than being conflated into a single term (as was possible for the muon and tau channels by their linearity on the imaginary component). This correction acts on both the muon and the tau channel to yield

$$\theta_e(\mathcal{E}) = -\frac{3\pi}{4} \left( 1 - \frac{4\sqrt{\delta_e\{r[\Delta_e(m_\tau, \mathcal{E}) - \Delta_e(m_\mu, \mathcal{E})]\}}}{3\pi} \right) \times \left( 1 + \frac{4\sqrt{\delta_e\{r[\Delta_e(m_e, \mathcal{E})]\}}}{3\pi} \right). \quad (101)$$

#### IV. RELATIONSHIPS FROM $\mathbb{R}^{0|18}$ DUST GRAVITY

##### A. Mass relationships

To obtain testable predictions from  $\mathbb{R}^{0|18}$  dust gravity, it is necessary to eliminate the model parameters

$f$ ,  $\mathcal{E}_{\text{QL}}^{(1)}$ , and  $\mathcal{E}_{\text{QL}}^{(2)}$  from the mass expressions derived above. This is readily achieved by taking ratios of particle masses. Recognising that the choice of gauge articulated in Sec. III C 5 fixes the value of  $m_e^2$  so this does not run with energy scale, the value of  $m_\tau^2(\mathcal{E}_\tau)/m_e^2(\mathcal{E}_\tau)$  evaluated at energy scale  $\mathcal{E}_\tau = m_\tau c^2$  then readily admits interpretation as the ratio of the rest masses of the electron and the tau, and similarly for  $m_\mu^2(\mathcal{E}_\mu)/m_e^2(\mathcal{E}_\mu)$  and the rest mass of the muon.

In conjunction with the boson mass expressions developed in Sec. II, and noting the freedom to substitute

$$\frac{m_e^2}{[k_1^{(e)}(\mathcal{E}_e)]^4} \rightarrow \frac{m_\mu^2}{[k_2^{(e)}(\mathcal{E}_\mu)]^4} \quad (102)$$

or

$$\frac{m_e^2}{[k_1^{(e)}(\mathcal{E}_e)]^4} \rightarrow \frac{m_\tau^2}{[k_3^{(e)}(\mathcal{E}_\tau)]^4} \quad (103)$$

as convenient, as discussed in Sec. II A 2, this yields the relationships (at the present level of precision)

$$\frac{m_\tau^2}{m_e^2} = \frac{[k_3^{(e)}(\mathcal{E}_\tau)]^4 \left\{ 1 + \frac{90\alpha m_\tau^2}{\pi[m_c^*(\mathcal{E}_\tau)]^2} + \frac{(5-4f_Z)\alpha m_\tau^2}{2\pi m_W^2} + \frac{5m_\tau^2}{[m_c^*(\mathcal{E}_\tau)]^2} \left[ 1 + \frac{90\alpha m_\tau^2}{\pi[m_c^*(\mathcal{E}_\tau)]^2} + \frac{(25-12f_Z)\alpha m_\tau^2}{6\pi m_W^2} \right] + \frac{240m_\tau^4}{[k_3^{(e)}(\mathcal{E}_\tau)]^4 m_{\text{H}'}^2 m_W^2} \right\}}{[k_1^{(e)}(\mathcal{E}_\tau)]^4 \left\{ 1 + \frac{90\alpha m_e^2}{\pi[m_c^*(\mathcal{E}_\tau)]^2} + \frac{(5-4f_Z)\alpha m_e^2}{2\pi m_W^2} + \frac{5m_e^2}{[m_c^*(\mathcal{E}_\tau)]^2} \left[ 1 + \frac{90\alpha m_e^2}{\pi[m_c^*(\mathcal{E}_\tau)]^2} + \frac{(25-12f_Z)\alpha m_e^2}{6\pi m_W^2} \right] + \frac{240m_e^2 m_\tau^2}{[k_3^{(e)}(\mathcal{E}_\tau)]^4 m_{\text{H}'}^2 m_W^2} \right\}} \quad (104)$$

$$\frac{m_\mu^2}{m_e^2} = \frac{[k_2^{(e)}(\mathcal{E}_\mu)]^4 \left\{ 1 + \frac{90\alpha m_\mu^2}{\pi[m_c^*(\mathcal{E}_\mu)]^2} + \frac{(5-4f_Z)\alpha m_\mu^2}{2\pi m_W^2} + \frac{5m_\mu^2}{[m_c^*(\mathcal{E}_\mu)]^2} \left[ 1 + \frac{90\alpha m_\mu^2}{\pi[m_c^*(\mathcal{E}_\mu)]^2} + \frac{(25-12f_Z)\alpha m_\mu^2}{6\pi m_W^2} \right] + \frac{240m_\mu^4}{[k_2^{(e)}(\mathcal{E}_\mu)]^4 m_{\text{H}'}^2 m_W^2} \right\}}{[k_1^{(e)}(\mathcal{E}_\mu)]^4 \left\{ 1 + \frac{90\alpha m_e^2}{\pi[m_c^*(\mathcal{E}_\mu)]^2} + \frac{(5-4f_Z)\alpha m_e^2}{2\pi m_W^2} + \frac{5m_e^2}{[m_c^*(\mathcal{E}_\mu)]^2} \left[ 1 + \frac{90\alpha m_e^2}{\pi[m_c^*(\mathcal{E}_\mu)]^2} + \frac{(25-12f_Z)\alpha m_e^2}{6\pi m_W^2} \right] + \frac{240m_e^2 m_\mu^2}{[k_2^{(e)}(\mathcal{E}_\mu)]^4 m_{\text{H}'}^2 m_W^2} \right\}} \quad (105)$$

$$\frac{m_W^2}{m_Z^2} = \frac{3 \left[ 1 + \left( 64 + \frac{3}{2\pi} - f_Z \right) \frac{\alpha}{2\pi} \right] \left\{ 1 + \frac{19m_\mu^2}{[k_2^{(e)}(\mathcal{E}_\mu)]^4 m_W^2} \right\}}{4 \left[ 1 + \left( \frac{401}{12} + \frac{3}{2\pi} \right) \frac{\alpha}{2\pi} \right] \left\{ 1 + \frac{23m_\mu^2}{[k_2^{(e)}(\mathcal{E}_\mu)]^4 m_W^2} \right\}} \quad (106)$$

$$\frac{m_{\text{H}'}^2}{m_W^2} = \frac{20 \left( 1 + \frac{1}{2\pi} \right) \left( 1 + \frac{6\alpha}{\pi} \right)}{9 \left[ 1 + \left( 64 + \frac{3}{2\pi} - f_Z \right) \frac{\alpha}{2\pi} \right] \left\{ 1 + \frac{19m_\mu^2}{[k_2^{(e)}(\mathcal{E}_\mu)]^4 m_W^2} \right\}} \quad (107)$$

$$\frac{m_c^2}{m_W^2} = \frac{1 + \frac{99m_\mu^2}{[k_2^{(e)}(\mathcal{E}_\mu)]^4 m_W^2}}{1 + \frac{19m_\mu^2}{[k_2^{(e)}(\mathcal{E}_\mu)]^4 m_W^2}} \quad (108)$$

where

$$k_n^{(\ell)}(\mathcal{E}) = 1 + \sqrt{2} \cos \left[ \theta_\ell(\mathcal{E}) - \frac{2\pi(n-1)}{3} \right] \quad (52b)$$

$$f_Z = \frac{1}{3} \left( 4 - 24 \frac{m_W^2}{m_Z^2} + 16 \frac{m_W^4}{m_Z^4} \right) \quad (19b)$$

$$[m_c^*(\mathcal{E})]^2 = m_c^2 \left( 1 - \frac{27}{10} \frac{\mathcal{E}^2}{m_c^2 c^4} \right) \quad (59b) \quad \text{and}$$

$$\mathcal{E}_\ell = m_\ell c^2 \quad (109)$$

---


$$\theta_e(\mathcal{E}) = -\frac{3\pi}{4} \left( 1 - \frac{4\sqrt{\delta_e \{r[\Delta_e(m_\tau, \mathcal{E}) - \Delta_e(m_\mu, \mathcal{E})]\}}}{3\pi} \right) \left( 1 + \frac{4\sqrt{\delta_e \{r[\Delta_e(m_e, \mathcal{E})]\}}}{3\pi} \right) \quad (101)$$

$$\Delta_e(m_{e_i}, \mathcal{E}) = \frac{90\alpha m_{e_i}^2}{\pi [m_c^*(\mathcal{E})]^2} + \frac{(5 - 4f_Z)\alpha m_{e_i}^2}{2\pi m_W^2} + \frac{5m_{e_i}^2}{[m_c^*(\mathcal{E})]^2} \left[ 1 + \frac{90\alpha m_{e_i}^2}{\pi [m_c^*(\mathcal{E})]^2} + \frac{(25 - 12f_Z)\alpha m_{e_i}^2}{6\pi m_W^2} \right] + \frac{240m_{e_i}^2 m_\mu^2}{[k_2^{(e)}(\mathcal{E}_\mu)]^4 m_{H'}^2 m_W^2} \quad (98)$$

$$r(n) = n \cdot \sqrt{1 + \frac{(1+n)^{-1} - 1}{9}} \quad (96)$$

$$\delta_e(n) = \sqrt{1 + \frac{\pi^2 n}{8} \left[ 1 + \frac{\pi^2 n}{32} \right]} - 1. \quad (92)$$

The lower precision on  $m_{H'}$  compared with the other weak bosons is acceptable as the main sensitivity to these higher-order mass corrections is in the lepton mass ratios via  $\theta_e$ , in which  $m_{H'}$  plays only a very small part. The terms provided suffice to calculate  $m_{H'}^2$  to current experimental precision.

Taking  $m_e$ ,  $m_\mu$ , and  $\alpha$  as input parameters [7, 8],

$$m_e = 0.5109989461(31) \text{ MeV}/c^2 \quad (110)$$

$$m_\mu = 105.6583745(24) \text{ MeV}/c^2 \quad (111)$$

$$\alpha = 7.2973525693(11) \times 10^{-3}, \quad (112)$$

these relationships may be solved numerically to yield the results given in Table II.

Parameter	Calculated value (GeV/ $c^2$ )	Observed value (GeV/ $c^2$ )	Discrepancy
$m_\tau$	1.776867(1)	1.77686(12)	0.06 $\sigma_{\text{exp}}$
$m_W$	80.3786(3)	80.379(12)	0.03 $\sigma_{\text{exp}}$
$m_Z$	91.1877(4)	91.1876(21)	0.05 $\sigma_{\text{exp}}$
$m_{H'}$	125.16(1)	125.10(14)	0.45 $\sigma_{\text{exp}}$
$m_c$	80.4276(4)	–	–

TABLE II. Calculated values of particle masses in  $\mathbb{R}^{018}$  dust gravity. Quantity  $m_c$  is the bare gluon mass. The displayed uncertainties in calculated masses arise from estimates of higher-order terms. The leading corrections due to uncertainty in  $m_e$ ,  $m_\mu$ , and  $\alpha$  are smaller, being of order  $10^{-3} \sigma_{\text{exp}}$ , or parts in  $10^7$  on all masses. The gluon mass shown is the bare mass at scales below  $\mathcal{E}_\psi$ , though with the caveat that it frequently becomes massless in interactions above this scale, as seen in the calculations above.

---

## B. Minimum requirements for particle generations from preon substructure

These results strongly suggest that particle generations arise from a preonic substructure for leptons. It would appear that the minimum requirements for direct import of this structure from  $\mathbb{R}^{018}$  dust gravity into a modification of the Standard Model while retaining its predictive capacity are as follows:

- A tripartite preon structure for leptons bound by a  $\text{GL}(3, \mathbb{R})$ -symmetric force sector [which need not necessarily correspond to the strong force plus an additional (axion?) companion, as here].
- A bipartite preon structure for the Higgs/scalar boson.
- A duality between preon/antipreon pairs and the electroweak and preon-binding bosons.
- A multi-species quantum liquid in place of the present nonvanishing vacuum expectation value of the Higgs boson.

However, these features come with costs, including:

- Importing the quantum liquid relegates the scalar boson to a bystander having only a small role to play in generating particle mass. The Higgs mechanism might still be responsible generating the quantum liquid, but will require some modification to be applied in this context.
- If the preon binding bosons are the gluons of the strong force, there must exist an axion (this may be useful as a dark matter candidate).
- If the preon binding bosons are not the gluons of the strong force, further work is required to determine whether the inhomogeneous preon triplets correspond to quarks and why they carry colour charge.

Alternatively the current role for the Higgs boson may be retained, but only at the cost of introducing numerous fine tuning parameters. Unless an alternative but equivalent mechanism for fixing these parameters is constructed, this comes at the cost of predictive power.

Although  $\mathbb{R}^{0|18}$  dust gravity incorporates a colour-based mechanism for particle generations with substantial predictive power in the electroweak sector, it is premature to identify this with electrostrong unification without at least some evidence of predictive capacity in the strong nuclear sector. It is, however, clearly a candidate for a unifying mechanism, and an obvious test would be calculation of the quark masses.

Multiple other avenues for further testing of  $\mathbb{R}^{0|18}$  dust gravity exist, both theoretical and experimental, and perhaps one of the most accessible relates to the weak mixing angle. In Eq. (37), the mass ratio used to compute  $\sin^2 \theta_W$  effectively takes a weighted average over all interactions of the  $Z$  boson, whereas in Sec. II C it is noted that differences in higher-order corrections which depend on fermion charge could result in differing electroweak couplings for different species, and thus different measured values of  $\sin^2 \theta_W$ . There do appear to be some discrepancies in the values of  $\sin^2 \theta_W$  measured using different species [9, p. 172], and it would be fruitful to assess whether this can be explained using  $\mathbb{R}^{0|18}$  dust gravity.

## V. CONCLUSION

$\mathbb{R}^{0|18}$  dust gravity is a model having many elements in common both with the Standard Model of particle physics and with the observable universe. As it has only four tunable parameters, which must be set by reference to physical constants,  $\mathbb{R}^{0|18}$  dust gravity may readily be tested against observation.

In the present paper, relationships in the electroweak sector of  $\mathbb{R}^{0|18}$  dust gravity were used to predict the values of several fundamental particle masses in the Standard Model, with results in excellent agreement with observation. These results arise from the particle generation mechanism used in  $\mathbb{R}^{0|18}$  dust gravity.

### Appendix A: Gell-Mann matrices

When working with the group  $SU(2)$ , a well-known basis for the tangent Lie Algebra  $\mathfrak{su}(2)$  is given by the

Pauli matrices  $\sigma_i$ , rescaled by a factor of  $1/\sqrt{2}$ :

$$\{\tau_i \mid i \in \{1, 2, 3\}\} \quad \tau_i = \frac{\sigma_i}{\sqrt{2}}. \quad (\text{A1})$$

A similar basis for  $\mathfrak{su}(3)$  is provided by rescaling the Gell-Mann matrices  $C_a$ ,

$$\{\lambda_i \mid i \in \{1, \dots, 8\}\} \quad \lambda_i = \frac{C_i}{\sqrt{2}} \quad (\text{A2})$$

where

$$\begin{aligned} C_1 &= \begin{pmatrix} 0 & 1 & 0 \\ 1 & 0 & 0 \\ 0 & 0 & 0 \end{pmatrix} & C_2 &= \begin{pmatrix} 0 & -i & 0 \\ i & 0 & 0 \\ 0 & 0 & 0 \end{pmatrix} \\ C_3 &= \begin{pmatrix} 1 & 0 & 0 \\ 0 & -1 & 0 \\ 0 & 0 & 0 \end{pmatrix} & C_4 &= \begin{pmatrix} 0 & 0 & 1 \\ 0 & 0 & 0 \\ 1 & 0 & 0 \end{pmatrix} \\ C_5 &= \begin{pmatrix} 0 & 0 & -i \\ 0 & 0 & 0 \\ i & 0 & 0 \end{pmatrix} & C_6 &= \begin{pmatrix} 0 & 0 & 0 \\ 0 & 0 & 1 \\ 0 & 1 & 0 \end{pmatrix} \\ C_7 &= \begin{pmatrix} 0 & 0 & 0 \\ 0 & 0 & -i \\ 0 & i & 0 \end{pmatrix} & C_8 &= \frac{2}{\sqrt{3}} \begin{pmatrix} \frac{1}{2} & 0 & 0 \\ 0 & \frac{1}{2} & 0 \\ 0 & 0 & -1 \end{pmatrix}. \end{aligned} \quad (\text{A3})$$

Like the rescaled Pauli matrices  $\tau_i$ , the re-scaled Gell-Mann matrices satisfy

$$\text{Tr}[(\lambda_i)^2] = 1 \quad \forall \quad i \in \{1, \dots, 8\}. \quad (\text{A4})$$

In conjunction with a multiple of the identity matrix

$$\lambda_9 = \frac{1}{\sqrt{3}} \begin{pmatrix} 1 & 0 & 0 \\ 0 & 1 & 0 \\ 0 & 0 & 1 \end{pmatrix}, \quad (\text{A5})$$

the matrices  $\lambda_i$  also yield a basis for  $\mathfrak{gl}(3, \mathbb{R})$ .

An alternative basis for  $\mathfrak{gl}(3, \mathbb{R})$  is given by the elementary matrices  $e_{ij}$ , consisting of a matrix with 1 in position  $(i, j)$  and zero elsewhere.

---

[1] R. N. C. Pfeifer, arXiv:0805.3819v14 (2020).  
[2] M. E. Peskin and D. V. Schroeder, "An Introduction to Quantum Field Theory," (Westview Press, USA, 1995) p. 773.  
[3] Y. Koide, in *Proc. 30th Int. Conf. High-energy Phys., Osaka, Japan*, edited by C. S. Lim and T. Yamanaka (World Scientific, Singapore, 2001) arXiv:hep-ph/0005137v1.

[4] R. Penrose, in *Combinatorial Mathematics and its Applications*, edited by D. J. A. Welsh (Academic Press, 1971) pp. 221–244.  
[5] R. N. C. Pfeifer, P. Corboz, O. Buerschaper, M. Aguado, M. Troyer, and G. Vidal, *Phys. Rev. B* **82**, 115126 (2010).  
[6] R. N. C. Pfeifer, *Simulation of Anyons Using Symmetric Tensor Network Algorithms*, Ph.D. thesis, The University

of Queensland (2011), arXiv:1202.1522v2.

- [7] P. A. Zyla *et al.*, to be published in *Prog. Theor. Exp. Phys.* **2020**, 083C01, (2020), <http://pdg.lbl.gov/>.
- [8] E. Tiesinga, P. J. Mohr, D. B. Newell, and B. N. Taylor, “The 2018 CODATA Recommended Values of the Fundamental Physical Constants,” (2018), (Web Version 8.1).
- [9] M. Tanabashi *et al.* (Particle Data Group), *Phys. Rev. D* **98**, 030001 (2018).

Database developed by J. Baker, M. Douma, and S. Kotchigova. Available at <http://physics.nist.gov/constants>, National Institute of Standards and Technology, Gaithersburg, MD 20899.